Two-phase closed thermosyphons: a review of studies and solar applications

Davoud Jafari, Alessandro Franco, Sauro Filippeschi, Paolo Di Marco
Department of Energy, Systems, Territory and Constructions Engineering (DESTEC),
University of Pisa, Italy

Abstract

The use of the two-phase closed thermosyphons (TPCTs) is increasing for many heat transfer applications. This paper reviews the most recent published experimental and theoretical studies on the TPCT. After a description of the TPCT operating principle and the performance characteristics, the heat transfer analysis in condenser and evaporator sections that depends on the complex two-phase process are described. The influence of the affecting parameters on the performance of TPCTs such as the geometry (diameter, shape and length), the inclination angle, the filling ratio (FR), the working fluid, the operating temperature and pressure analyzed by various researchers is discussed. The various operating limits occurring in a thermosyphon includes viscous, sonic, dryout, boiling and flooding are analyzed. Considering the application of TPCTs, the paper presents a review of experimental tests and applications. This paper can be used as the starting point for the researcher interested in the TPCTs and their renewable energy applications.

Keywords: Two-phase closed thermosyphon, renewable energy, heat transfer, operating limits, numerical modeling, experimental analysis, solar collectors

Corresponding Author:

Davoud Jafari
Department of Energy, Systems, Territory and Constructions Engineering (DESTEC), University of Pisa, Largo Lucio Lazzarino, 2, 56126 PISA, Italy
Phone: +390502217134
Email: d.jafari@studenti.unipi.it

Nomenclature

AR	aspect ratio, L_e/d_i
Ar	Archimid number, $(gd_i^3/v_l^2)^2(1-\rho_v/\rho_l)$
Bo	Bond number, d_i/L_b
c	specific heat (J/kg K)
d	diameter (m)
d_b	bubble departure diameter (m)
FR	filling ratio
Fr	Froude number, $(q/\rho_l h_{fg})[\rho_l/d_i g(\rho_l-\rho_v)]$
g	gravitational acceleration (m/s^2)
h	heat transfer coefficient (W/m^{2}K)
h_{fg}	heat of vaporization (J/kg)
Ja	Jacob number, $h_{fg}/C_{p,l}T_v$
k	thermal conductivity (W/mK)
L	length (m)
L^*	characteristic length (m) , $\left[v_l^2/g(\rho_l/\rho_l-\rho_v)\right]^{1/3}$
L_b	bubble length scale (m), $\left[\sigma/g(\rho_l-\rho_v)\right]^{1/2}$
$\dot{m}$	mass flow rate (kg/s)
Nu	Nusselt number, hL/k
Nu^*	modified Nusselt number, $Nu^* = h_c L^*/k_l$
P	pressure (Pa)
Pr	Prandtl number, v/α
Q	heat transfer rate (W)
q	heat flux (W/ m^2)
R	thermal resistance (K/W)
r	radius (m)
Ra	Rayleigh number, $g\beta q l_p^4/\alpha_l v_l k_l$
Re	Reynolds number, $4Q/\pi Dh_{fg}\pi$
R_g	gas constant (J/kg K)
T	temperature (K)
V	velocity (m/s)
We	Weber number, $\rho V^2 L/\sigma$

Greek symbols

α	diffusion coefficient (m^2/s)
β	inclination angle (˚)
v	kinematic viscosity (m^2/s)
ρ	density (kg/m^3)
μ	dynamic viscosity (Pa s)
σ	surface tension (N/m)
θ	contact angle (˚)

Subscripts

a	adiabatic
atm	atmospheric
c	condenser
crit	critical
e	evaporator
eff	effective
f	liquid film
i	inner
l	liquid
max	maximum
min	minimum
NB	nucleate boiling
o	outer
p	pool
sat	saturation
t	total
TPC	two-phase convection
v	vapor

1. Introduction

Heat pipes (HPs) have emerged as the most appropriate technology and cost effective thermal control solution due to their excellent heat transfer capabilities [1,2]. Interesting connection can be evidenced in the literature between HPs and thermal engineering applications [3]. A special HP where the condensed liquid moves to the condenser by gravity is two-phase closed thermosyphon (TPCT). In this device no capillary structure is present and it works in a two-phase close cycle where latent heat of evaporation and condensation is used to transfer heat. The TPCT can work in gravity [4] or antigravity mode with the condenser above the evaporator [5]. In this last case the system operates in an unsteady, e.g. periodic regime. There are other kinds of two-phase thermosyphon systems such as two-phase closed loop thermosyphons (TPCLTs) [6] and two-phase microchannel thermosyphon [7].

A TPCT can be used in much wider thermal and temperature ranges than a wicked HP, since it does not have the large flow resistance or low boiling limit inside the wick, as the condensate liquid in the TPCT is returned to the heated side of the system under the effect of gravity, instead of capillary forces in wicked HPs [8]. However, TPCTs have major limits on the maximum amount of thermal energy that can be transferred due to viscous, sonic, dryout, flooding and entrainment limits [9].

The TPCT technology has found increasing interest of the researchers in a wide range of applications from small-scale to large-scale systems. TPCTs are used in chemical and petroleum industries applications [10], electronic cooling [11,12], telecommunication devices [13], energy storage systems [14], the railway transportation systems [15], thermoelectric power generators [16], seasonal cooling load reduction of buildings [17], cooling of super conducting bearings [18] and various heating and cooling applications [19]. TPCTs can be also used for thermal control in particular in connection with solar energy systems like solar collectors [20] or photovoltaic systems [21]. A general description of TPCT systems is reported in **Fig. 1.**

The widely spread use of TPCTs has led to increase the demand for analytical and numerical models and predictive tools that would allow the thermal engineers to predict their performance. There are experimental studies which have tried to predict the complex mechanism inside the TPCT. Although considerable studies have been undertaken to investigate the behavior of the TPCT in steady operating conditions, there still exists considerable uncertainty in the description of the complex physical phenomena of TPCTs. The heat and mass

transfer through a TPCT is, in fact, significantly affected by different parameters and design variables such as: geometry, inclination angle, filling ratio (FR), thermophysical properties of working fluid, and vapor temperature and pressure. The large number of physical parameters affecting the TPCT performances has, therefore, prevented a complete understanding of the mechanisms of the heat and mass transfer in the TPCT and the possibility of analyzing the system performance under a variety of operating conditions and design variables. This complex mechanisms include: wall and interfacial heat transfer; thin film flows, interfacial mass transfer, compressible vapor effects and phase-change phenomena (boiling, condensation and evaporation).Considering the above, the present review outlines the state-of-the-art of TPCT technology, design methodologies and applications. The paper is organized into two main sections: thermal analysis of TPCTs and applications. The first section is divided into five different parts: background and operating principle, heat transfer analysis, analytical and numerical approaches, operating limit, and experimental devices. The second section analyzes the applications with specific attention to recent published renewable energy application including: solar applications and air to air heat exchangers.

2. TPCT: Background and operating principle

The main physical mechanisms of a TPCT are easily understood by using the scheme shown in **Fig. 2(a)**. Basically, TPCTs consist of three different sections: an evaporator, a condenser and an adiabatic section. To determine the TPCT performance, it is necessary to know the thermal-fluid phenomena occurring inside it. In such a device, the input power is supplied through the evaporator wall to the working fluid and the liquid contained in the pool inside the evaporator starts to evaporate. Vapor flows upward inside the pipe up to the condenser which is condensing the working fluid at the inner pipe wall (reflux condensation). Film condensation starts at the condenser inner walls and film thickness hardly affects the fluid dynamics of vapor flow in the core region of thermosyphon. In cases of a low vapor velocity, a liquid film increases its thickness downwards (due to gravity) counter currently to the vapor. As the vapor velocities increase, however, interactions between the liquid and vapor bring out critical situations which result in a heat transfer limit, named flooding limit [1]. The different heat and mass transfer processes occurring inside a TPCT are: convection, pool boiling, thin liquid film evaporation, counter current two-phase flow and filmwise condensation. In order to have a better understanding

of the heat transfer inside a TPCT under steady-state conditions, a classical thermal network scheme is presented in **Fig. 2(b)** as well as the expression for different resistances of the thermal circuit.

As discussed earlier, the thermal–hydraulic behavior in a TPCT is determined by various operating parameters: the input heat, the FR, the working fluid and the pipe geometry (diameter, length, inclination angle and shape of the cross-section). The geometry of pipe is one of the important parameters. The heat transfer and the motion in a two-phase system can be strongly influenced by the pipe diameter. Diameter gives reason of the balance among inertial, capillary and gravity forces. The relative importance of inertial and capillary forces is indicated by the Weber number (*We*). If *We* >> 1, inertia forces dominate the behaviour. The relative importance of inertia and gravity (body) forces are indicated by the Froude number (*Fr*). If *Fr* >> 1, inertia forces are dominant compared to gravity forces. The ratio between *We* and *Fr* defines the Bond number (*Bo*). Bo can be defined as the ratio of buoyancy force over surface tension force which can rule boiling phenomena inside the evaporator section and the size of vapor bubbles occurring in nucleate boiling. The value of *Bo* primarily affects the maximum heat transfer capacity in the evaporator section. The change of *Bo* value depends on two main parameters: the density of working fluid and diameter of the TPCT. Thus, the *Bo* can be considered as an indicator for the connection between two-phase flow pattern and pipe diameter.

As mentioned by Franco and Filippeschi [4], the minimum tube diameter ($d_{crit,\min}$) to obtain bubble development and plug/slug or slug flow in the pipe is $d_{crit,min}=2L_b$, where L_b is the bubble length scale. This is confirmed also by Jouhara and Robinson [22], who claim that the condition for the TPCT to be considered small can be described as the condition whereby the expected bubble departure diameter (d_b)is about the half of the diameter the pipe, $d_i=2d_b$, where d_b is directly depend on the contact angle (θ) and the bubble length, $d_b=f(\theta,L_b)$. Franco and Filippeschi [23] experimentally analyzed the behavior of the complete system which is strongly influenced by the type of flow and the diameter of the pipe. They observed in particular that the size of the pipe mainly in the evaporation zone is of particular importance so that the devices could be divided in high *Bo*, where the effects of surface tension can be neglected and low *Bo*, in which the forces due to surface tension cannot be neglected at all.

3. TPCT: Heat transfer analysis

Before analyzing the analytical and numerical study on the TPCTs, the evaporation and condensation phenomena need to be described. The good performance of TPCTs mainly depends on the behaviour in evaporation and condensation sections. In this section, detailed analysis of condensation and evaporation heat transfer is presented. The most important published semi-empirical correlations for the definition of the HTC are analyzed and compared with the experimental data available in the literature.

3.1. Condensation heat transfer: analysis of the phenomena and experimental results

The condensation HTC in a TPCT is determined by both the falling film and the countercurrent vapor flow. There are some parameters that affect the HTC: thermal and hydrodynamic properties of the working fluid, local flow velocity, inclination angle and operating pressure and temperature. The complexity of the condensation process can be reduced according to Nusselt's theory to a rather simple model, namely that the resistance for the removal of the heat released during condensation occurs in the condensate film for a vertical wall. This is the first basic approach to the analysis of the HTC [24]. Rohsenow [25] modified the Nusselt correlation and tested it with experimental data for water. **Table 1** summarizes the main correlations for the determination of the condensation HTC in the literature. The researchers by extending the Nusselt theory and considering the laminar and turbulent flow and the countercurrent vapor-liquid for a TPCT concluded that for the case of a laminar film flow, the effect of interfacial shear on the film flow is very small and therefore the classical Nusselt solution is adequate for the prediction of results [26,27]. Therefore, the HTC in the condenser region of the TPCTs is generally predicted using Nusselt theory. Another interesting approach that modified the Nusselt theory is given by [28] who indicated that agreement between measurements and Nusselt theory is not assured for all the conditions. Thus, he defined a modified correlation.

For vertical downward co-current vapor and condensate film flow, a significant amount of experimental data and correlations are available in [29]. Different approaches for defining the HTC can be observed in Wang and Ma [30]. They carried out theoretical and experimental analysis on vertical and inclined TPCTs (d_i=20 mm and L=1800 mm) with water as a working fluid and presented a semi-empirical correlation for condensation heat transfer by considering the influence of the inclination angle (β). In a similar approach, Fiedler and Auracher

[31] experimentally investigated the reflux condensation of R134a as working fluid in an inclined small diameter pipe (d_i=7 mm and L=500 mm). A comparison of the experimental results with values predicted by the classical Nusselt theory show that it underpredicts the experimental values for the vertical position. They modified suggested correlation by [30] to predict the average HTC in dependence of the inclination angle. Hussein et al. [32] presented a steady state 2-D theoretical analysis of laminar film condensation heat transfer inside the condenser section in case of an inclined thermosyphon. They presented a correlation that is in good agreement with the experimental results for a wide range of inclination angles. Hashimoto and Kaminaga [33] experimentally investigated condensation heat transfer due to fluid entrainment in a TPCT for water, ethanol and R-113 as a working fluid. They found that the condensation heat transfer values are smaller than those calculated from the Nusselt theory, mainly when working fluid entrainment occurs. Thus, they proposed a correlation that takes into account the fact that at lower heat fluxes the film thickness is smaller, combined with the knowledge that the amount of entrainment increases as the density ratio increases (ρ_l/ρ_v). Jouhara and Robinson [22] experimentally investigated the performance of a TPCT using water, FC-84, FC-77 and FC-3283. In the condenser section, the experimental data were close to the trend defined by [33]; however they observed that the liquid entrainment affects the condensation heat transfer for low power levels, thus a modification has been proposed with introduction of the constant 0.14 instead of 0.6. Oh and Revankar [34] experimentally studied steam condensation in a vertical pipe (d_i=26 mm and L=980 mm) by using a modified Nusselt correction ($h_c=1.2h_{Nusselt}$). The experiments were performed for the HTC and heat flux ranges of 6-1210 kW/m^{2}K and 36-120 kW/m^2, respectively. They showed that for low film Reynolds number and low interfacial shear conditions, the modified Nusselt model agrees well with the experimental data. Gross and Philipp [35] experimentally investigated conjugated shear stress and Prandtl number effects on reflux condensation heat transfer inside a vertical pipe (d_i=28 mm and L=4200 mm) with water, ethanol and isopropanol as a working fluid. They did not propose a correlation, but they concluded that that the Nusselt theory and simple modification of the model is only valid for selected cases with an extremely thin film and the deviations from the experimental results rapidly increase with rising film thickness and shear stress. Baojin et al. [36] investigated heat transfer characteristics of titanium and copper TPCT with water as working fluid. Experimental results show that there are no remarkable differences of the HTC in evaporator between the two kinds of TPCTs, whereas surprisingly the experimental

results of the HTC in the condenser of the titanium-water system are about 2–3 times more than that of copper-water one. Moreover, they found that the Nusselt's theoretical correlation based on laminar filmwise condensation is not suitable for simulating the titanium-water TPCTs.

3.2. Evaporation heat transfer: analysis of phenomena and experimental results

The analysis of the heat transfer phenomena in the evaporator also is important. The working fluid inside the evaporator shows three behaviors, mainly the liquid pool, the liquid film and the vapor. Therefore, the heat transfer mechanism at the evaporator section is complex. Various heat transfer regimes can be observed: natural convection (at low heat fluxes), mixed convection (at intermediate heat fluxes) and the nucleate boiling (at high heat fluxes); the occurrence of one of the different regimes depends on the complex combination of geometry, the FR and the heat flux. Natural convection regime has received less attention in the thermosyphon applications due to its relatively low HTC. El-Genk and Saber [37] proposed the use of the following correlation for natural convection regime:

$$h_{nat} = 0.475\left(\frac{k_l}{L_p}\right)Ra^{0.35}\left(\frac{L_b}{d_i}\right)^{0.58} \quad (1)$$

The conventional nucleate boiling heat transfer correlations are not directly applicable because they do not take into account the effect of local mixing along the heated wall between the sliding bubbles and in the pool by departing and rising bubbles. For a small FR, the convective boiling and the evaporation at the condensate film returning to the evaporator is a dominating heat transfer mechanism. However, as the FR increases nucleate boiling is the dominant heat transfer mechanism in the evaporator. The main available correlations for the nucleate boiling regime (Rohsenow [24], Kutateladze correlation [24], Stephan and Abdelsalam [38], Imura et al. [39], Shiraishi et al. [40], Chowdhury et al. [41], El-Genk and Saber [37] and Kiatsiriroat et al. [42]) are summarized in **Table 2**, even if various other correlations exist in the literature [24,29]. Jouhara and Robinson [22] summarized some of the nucleate pool boiling correlations, in particular those occurring frequently in thermosyphon publications, and compared with their experimental results. There is no unique correlation that is sufficient to define the nucleate pool boiling HTC in all thermosyphons. It is common to choose one or more boiling correlations to compare the obtained results with the experimental data. In order to select the most

appropriate heat transfer correlations during operation El-Genk and Saber [37] proposed a criterion to define the heat transfer regime inside the pool, based on dimensionless parameter

$$X = \Psi\left(Ra \ \ \mathrm{Pr}_l\right)^{0.35}\left(\frac{P_v L_b q}{\sigma \rho_g h_{fg} \nu_l}\right)^{0.7} \tag{2}$$

where X is the dominant heat transfer regime and Ψ is the mixing coefficient (see **Table 2**). Heat transfer of the pool is dominated by natural convection if $X < 10^6$. Two-phase convection is considered if $10^6 \le X \le 2.1\times10^7$ while nucleate boiling is considered if $X > 2.1\times 10^7$. The criterion proposed in [37] is considered in recent paper [43] for the transition values. In particular, they suggested following correlation for two-phase convection (h_{TPC}) and transition between two-phase convection and nucleate boiling ($h_{TPC\text{-}NB}$):

$$h_{TPC} = 4\left(\frac{k_l}{d_i}\right)\left(ArFr^{0.5}\right)^{1/3}\mathrm{Pr}_l^{0.5}\left(\frac{Bo}{10}\right)^n, n = \begin{cases}1/2, \text{For} & Bo \le 10\\ 1/6, \text{For} & Bo \ge 10\end{cases}, \quad 10^6 \le X \le 2.1\times 10^6 \tag{3}$$

$$h_{TPC-NB} = \left(\frac{10}{8} - \frac{X}{8\times10^6}\right)^{3/4} h_{TPC} + \left(\frac{X}{8\times10^6} - \frac{2}{8}\right)^{3/4} h_{NB}, 2.1\times10^6 \le X \le 10^7 \tag{4}$$

Considering the experimental investigation in the evaporator zone of a TPCT, Chowdhury et al. [41] investigated a TPCT using ethanol, Freon R-113 and water as a working fluid. They considered the dependency of boiling heat transfer on pressure by introduction of a density ratio (ρ_v/ρ_l). They presented a correlation for each fluid. A correlation for definition of the HTC in nucleate boiling regime is proposed by El-Genk and Saber [37]. They tested different fluids: water, ethanol, methanol, Dowtherm-A, R-11 and R-113 in small cylindrical enclosures. The data covered a wide range of diameters (6-37 mm) and heated pool heights (50-800 mm). The proposed correlation showed good agreement with the experimental data, within a range of ±15%. Kiatsiriroat et al. [42] experimentally studied the thermal performance of a TPCT using water, ethanol and triethylene glycol (TEG) with variations of mixing parameters. They concluded that at low temperature of the heat source, the ethanol–water mixture has a higher heat transfer rate than that of water and close to that of pure ethanol. In the case of TEG–water mixture, the heat transfer rate of the thermosyphon varies with the content of TEG in the mixture. They reported the use of a modified Rohsenow correlation to predict the boiling HTC inside the thermosyphon. Park et al. [44] investigated experimentally the effect of FR (10-70%) on the HTC of a TPCT with FC-72 as a working fluid and a heat input ranged 50–600W. The results are in good agreement with the Imura correlation.

Noie [45] experimentally analyzed the effects of the input heat transfer rate, FR, and the evaporator length on the heat transfer performance in a TPCT. They found that the condensation heat transfer increases as the FR increases and the maximum condensation HTC takes place at inclination angle of 30˚ and FR of 22% and 30%. While at inclination angle of 45˚ the maximum condensation HTC takes place at FR of 15%. Comparisons of HTC in the evaporator showed good agreement with predictions by Imura. Guo and Nutter [46] experimentally investigated the effect of axial conduction through the pipe wall on the performance of a TPCT with R134a as a working fluid and different FR. It was found that axial conduction through the pipe wall caused an increase in the evaporation and condensation HTC of the thermosyphon. The results showed good agreement with the Imura correlation for the evaporator section and Gross correlation for the HTC in the condenser section.

Pioro [47] experimentally justified the values of the constants in the Rohsenow nucleate boiling correlation by using different materials (copper, aluminum, brass and stainless steel) and working fluids (water, ethanol, R-113 and R-11). Pioro et al. [48] investigated the parameters affecting nucleate pool-boiling heat transfer for different fluids such as water, ethanol, R-113, and n-heptane and operating conditions. They found that the Rohsenow correlation is one of the most accurate among those assessed. Filippeschi and Salvadori [49] analyzed the transient boiling heat transfer regime in a two-phase thermosyphon system using the FC72 as working fluid. They showed that no nucleate boiling regime has been observed in the evaporator, which works in an unstable transitional boiling regime with relative HTCs lower than those typical of nucleate boiling regimes (lower than 50%). They did not propose a correlation, but they suggested some problems with the use of conventional correlations.

3.3. Comparative analysis of the heat transfer correlations with the experimental data

In this section, the utilization of the various correlations for the HTC in the condenser and evaporator sections of TPCTs in various experimental test rigs is analyzed. **Table 3** provides a synthetic overview of the various correlations joined with the experimental conditions. **Table 3** includes different pipe material (copper, stainless steel, titanium), working fluids (water, ethanol, R113, TEG, FC72, R134a), inside diameters (2.8 mm<d_i <25mm), aspect ratios (2<$AR=L_e/d_i$<22), filling ratio (10<FR<160) and also provides the ranges of heat fluxes,

thermal resistance and HTCs. It should be noted that all the experimental results are related to vertical TPCTs. A joined analysis of **Tables 1- 3** could be useful to suggest the use of a specific correlation for specific situations.

Figs. 3 and **4** present a comparison of the experimental HTCs to the results of calculations based on theoretical correlations. **Figs. 3(a**) and **3(b)** show the comparison of experimental and theoretical HTC values for the evaporator section for water and other working fluids (ethanol, TEG, R134a and FC72), respectively and HTCs lower that 10 kW/m^{2}K. Also, a comparison of the experimentally and theoretically determined HTC values for the evaporator section for water, ethanol and R113 at high HTC (20-70kW/m^{2}K) is given in **Fig. 3(c).** Further, **Figs. 4(a)** and **4(b)** show the comparison of experimental and theoretical HTC values for the condenser section for water and other working fluids (ethanol, TEG, R134a and FC72), respectively. The experiments and predictions are shown within the ±20% band. From the analysis of presented data, it can be found that the results appear to be dispersed both for condenser and evaporator sections. The main reasons for the difference between results could be due to: temperature measurement errors, heat losses of operating experiment and the different position of measurement points of saturation temperature (for example in some cases the measurement points are the outer wall of adiabatic section and in other cases inside the pipe). Most correlations can be recommended to predict the heat transfer coefficient for pool boiling on TPCTs within an acceptable error limit in the specific criteria. As is well known, the influence of pipe geometry and material and working fluid must be considered in a further analysis, since the correlations are valid for the range of parameters covered in the respective study.

4. TPCT: operating limit

Although TPCTs are very effective heat transfer devices, they are subject to a well-known number of operating limits: viscous, sonic, dryout, boiling and flooding and other phenomena called geyser boiling.

Sonic limit- For liquid metals as a working fluid, the vapor velocity can reach sonic levels in start-up or in steady-state conditions. After the sonic speed is reached, the vapor usually located in thermosyphon core, experiences a shock wave. This specific limit is considered in [1], but a practical evidenced has never been observed.

Viscous limit- For thermosyphons working at low temperature levels, the vapor pressure differences between the evaporator and condenser can be very small. If this pressure difference is smaller than the viscous forces, the vapor is not able to move and the viscous limit is reached [7].

Dryout limit- The dryout limitation occurs at a very small FR. The minimum mass of working fluid is required for the continuous circulation of vapor and liquid film. When the available fluid mass is smaller than the minimum for a given heat flux, the bottom of evaporator experiences dryout, which can cause dry spots to form on the heated surface of the walls of the evaporator [7,50,51].

Boiling limit- At relatively larger FRs and higher radial heat fluxes, the performance of a TPCT is usually restricted by the boiling limit. At the CHF, a transition from nucleate boiling to film boiling occurs. Film boiling in turn, causes a sharp decrease in heat transfer rates and greatly increases the risk of severe structural damage due to high temperatures [2].

Flooding limit- The latent heat of vaporization of the working fluid plays an important role in controlling the flooding limit (higher latent heat results in higher CHF). Flooding limit occur at large FRs and high axial heat fluxes, but small radial heat fluxes. Flooding occurs when the upward velocities of the vapor are high enough to prevent the liquid film from flowing back to the evaporator due to the shear stress at the interface of the countercurrent liquid-vapor flow. As a result, liquid drops are entrained from film to the vapor and transported to the condenser by vapor flowing with high velocity. Consequently, the evaporator can experience dryout resulting in a rise in wall temperature [2,44,52-54].

Geyser boiling phenomena- Among the other phenomena, it seem interesting to introduce geyser boiling which is an unstable phenomenon inside thermosyphon due to vapor that generates and expands suddenly due to hydraulic head reduction, and may cause vibration and damage of the pipes. The geyser boiling puts no limitation on thermal performance of thermosyphon, but it should be avoided because it damages the condenser end cap due to the slug impact [55-57]. Khazaee et al. [58] investigated the geyser boiling in two TPCTs (d_i=15, 25 mm and L=1000 mm). The experiment results showed that the period of geyser boiling decreased by increasing the heat load and aspect ratio and increased by increasing the FR.

4.1. Operating limits: modeling and experimental analysis

The most important limitations of the TPCTs can be grouped into two categories: dryout limit for small FR (less than about 30%) and flooding and boiling limit for large FR. The determination of the various operating limits can be explained by dimensionless approaches as well detailed in [1,2,7]. However, the use of dimensionless approaches is not sufficient to well understand implication of operating limits in some practical applications. In this section, we intend to present state of understanding and prediction capacity for CHF during operation, through both TPCT advanced modeling and experimental investigation. Zuo and Gunnerson [54] experimentally and numerically investigated a TPCT (d_i=19 mm and L=1800 mm) using water as working fluid. They investigated the dryout and flooding limiting mechanisms and observed that the model is capable of predicting the performance of an inclined thermosyphon. However, the comparisons between theoretical and experimental results were carried out for the flooding limit. They found that the highest flooding limit is at inclination angles ranging from 30-45°. El-Genk and Saber [50] developed a one dimensional, steady state model for determining the operation envelopes of TPCTs. The model calculated the length of the liquid film and expanding liquid pool in the evaporator as parametric function of dimensions, vapor temperature of working fluid and power input. The TPCT operation envelope was an enclosure with three boundaries (dryout, boiling, and flooding limits). The results showed that an increase in the evaporator length, diameter and vapor temperature expanded the operation envelope, whereas an increase in the length of the condenser or the adiabatic section only slightly changed the envelope's upper and lower boundaries. However, the model can not be used to investigate the effect of FR in normal operation. Jiao et al. [59] developed a steady state model to investigate the effect of the FR on the distribution of the liquid film and liquid pool. Three types of flow pattern and two types of transition were considered in the model, according to the distribution of liquid film and liquid pool (see **Fig. 5**). In the liquid pool model, natural convection and nucleate boiling were considered by combination of their effective areas and HTCs. They concluded that the model is beneficial for selecting the FR, according to structure parameter and operating pressure of a TPCT. They showed that as the pipe diameter increases the critical FR increases. Jiao et al. [51] developed the previous model to utilize the criteria for dryout, flooding and boiling limits to investigate the effects of FR. They introduced the concept of minimum filling ratio to predict dryout limit (the liquid film thickness in evaporator reaches the minimum value, below which liquid film could experience dryout), the

maximum Reynolds number of vapor flow at the exit of condenser was used for predicting flooding limit and an empirical value of void fraction was used for predicting boiling limit. The experiments with nitrogen as the working fluid were performed and the maximum FR was introduced. It was concluded that in the horizontal direction, flooding and boiling limits increase with operating pressure. Boiling limit is independent of condenser length, while flooding limit decreases as it increases. Also, as the pipe diameter increases, the three limits and the maximum FR all increase.

Before getting into description of the experimental analysis on the TPCTs, the most important flooding limit correlation (see **Table 4)** is discussed herein, because a large number correlations investigated deal with flooding limit. Some correlations are defined by a balance of inertial forces and depend on the pipe design (Wallis correlation) but the effect of surface tension is not considered. Other correlations do not consider the effect of diameter (Kutateladze correlation), however the effect of diameter must be considered for small pipe diameter, since vapor through the pipe plays an important role. The empirical Imura correlation modified the Kutateladze correlation by taking into account the ratio of density, however the effect of diameter is not considered. In the Tien and Chung correlation the Kutateladze and Wallis correlations were modified by considering both the effect of pipe diameter and the surface tension. Considering experimental investigation, Faghri et al. [60] investigated a TPCT (d_i=16 mm and L=1000 mm) using water as a working fluid. They presented a correlation for flooding limit considering the experimental results and the correlations of Tien and Chung and Imura (see **Table 4**). Katto and Hirao [61] experimental investigated the CHF of counter-flow boiling in a vertical pipe (open to an upper and closed at the bottom end) with inner diameters of 8 and 10 mm (L/d_i = 125). From the experimental results, they presented an empirical correlation for predicting the flooding limit in a vertical pipe. Golobic and Gaspersic [62] presented a method for predict the performance limit in a TPCT based on the thermodynamical corresponding states principle. Molecular weight, critical temperature, critical pressure and acentric factor were used instead of thermodynamic and transport properties of fluid. They reported fairly good agreement between the 436 experimental data points (12 nonpolar and polar fluids, filling ratio greater than 0.4, inner diameter of 3-34 mm and different aspect ratios) and different flooding correlations. In particular, they observed good agreement with the Katto and Hirao correlation for a different range of aspect ratio. Nakano et al. [63] experimentally investigated a TPCT filled with nitrogen (FR of 100%). The experimental results are validated

with a good agreement the theoretical prediction of Imura, Tien and Chung and Katto and Hirao. Kiatsiriroat et al. [42] found that the equation developed by [60] can be used to predict the CHF due to the flooding limit. Between different pipe diameters (12.7, 19 and 25 mm), they found the flooding limit to occur in a thermosyphon with d_i=12.7 mm. Park et al. [44] observed that for the small FR (less than 20%), the critical limitation is dryout, while for the large FR the flooding limitation occurred. They found the flooding limitation of 500–550 W for Bo=26–28 and 230 W for Bo=18.3, for the large FR. The experimental results showed good agreement with Wallis correlation at C_w=0.8. Payakaruk et al. [64] experimentally predicted heat transfer characteristics of TPCT (d_i=7.5, 11 and 25 mm). Different working fluids (R22, R123, R134a, ethanol, and water), FRs (50-100%) and the aspect ratios (5-40) were studied. It was found that, the FR has no effect on the ratio of heat transfer characteristics at any angle to that of the vertical position, but the properties of the HTF affected the heat transfer rate. They presented the following correlation for the ratio of maximum heat transfer rate at a given angle to that of vertical position (Q_m/Q_{90}):

$$\frac{Q_m}{Q_{90}} = 1.678\left\{\frac{q}{\rho_v h_{fg}\left[\sigma g\left(\frac{\rho_v-\rho_l}{\rho_v^2}\right)\right]^{0.25}}\frac{d_i}{L_e}\frac{\rho_v}{\rho_l}\right\}^{0.0196} \tag{5}$$

Liu et al. [65] investigated the effect of the inclination angle on the CHF of countercurrent boiling in an inclined uniformly heated tube with open top and closed bottom ends at zero inlet flow ($25<L_e/d_i<145$). The experimental results show that the CHF data of the small vertical tubes agree reasonably well with the predictions of the Tien and Chung correlation and decrease with reducing the inclination angle. Rittidech and Srimuang [66] experimentally determined the effect of dimensionless parameters on heat-transfer characteristics of a vertical flat thermosyphon with a copper pipe with an inner diameter of 8.6 mm. R123, ethanol and water were used as a working fluid with FRs of 20-80%. They observed that the heat transfer capacity of flat thermosyphon is higher than that of the circular one. They concluded that the maximum heat flux of the flat thermosyphon in the vertical position can be evaluated from the following correlation:

$$Q_m = 0.0144\rho_v h_{fg}\left[\sigma g\left(\frac{\rho_v-\rho_l}{\rho_v^2}\right)\right]^{0.25}\left[\left(\frac{L_e}{4R_h}\right)^{0.9} Bo^4\, Ja^{1.8}\,\mathrm{Pr}^2\left(\frac{\rho_v}{\rho_l}\right)^{1.8}\right]^{0.13} \tag{6}$$

Grooten and van der Geld [67] experimentally investigated a long thermosyphon (d_i=14.5 mm and L=3000 mm) with R-134a as working fluid. The effects of saturation temperature, FR, and angle of inclination on the operational limiting heat flux were investigated. They found that as the saturation temperature increases the maximum heat transfer capacity increases and the FR is found not to be critical if it exceeds 25%. They presented a correlation to predict the operation limiting heat flux for thermosyphons with a L_e/d_i ratio up to 188. Long and Zhang [68] experimentally investigated the heat transfer performance of a thermosyphon filled with helium as the working fluid. They showed that the heat transfer rate of the dryout limit rises with the increase of the FR and then it reaches a maximum value due to the limitation of the critical point of helium. They observed that the thermal resistance decreases with the increasing of the FR for the cases of the FRs lower than 80%, but it increases when FR is 100% or higher because of the geyser boiling. They showed that the dryout limit can be calculated by dryout correlation (see Table 4[7]) with satisfying accuracy ($\pm$ 15%) for the FR less than 100%. The CHF changes depending on the variation of geometry, orientation, working fluids and operating parameters etc., thus direct comparisons between the results are not possible. **Table 4** summarizes the main correlations for the determination of the heat transfer limits in the literature. **Table 5** shows an overview on experimental data that focuses on analyzing operating limits of TPCTs. As evidenced, a large number correlations and investigations deal with understanding CHF at high FR, due to flooding limit. **Fig. 6** presents a comparison of the experimental heat transfer rate versus the results of calculations based on theoretical correlations. In order to investigate the effect of Bond number on the maximum heat transfer rate, the ratio of the maximum heat transfer rate (Q_{exp}) to the heat transfer rate calculated ($Q_{predict}$) from correlations are plotted against the Bond number in **Fig. 7**. It may be concluded that the effect of Bo can not be recognized for selected working fluid (R134a, nitrogen and FC-72), except for small Bo. It suggests that the effect of bubbles on the heat transfer rate is small for large Bond numbers.

5. TPCT: Analytical and numerical approaches

The possible use of TPCTs for various heat transfer applications has led to an increased demand for complete predictive tools that would allow the thermal engineers to perform preliminary design and analysis of behaviour of TPCTs. In an effort to meet this demand, some investigators attempted to present modeling tools, ranging

from the simple lumped capacity models up to complex transient multi-dimensional simulation. To determine the heat capability through a TPCT and performance characteristics, it is necessary to know the thermal fluid heat and mass transfer mechanism occurring inside a TPCT (see sections 2-4). The complex phenomena must be joined together; however, in a real application, several assumptions and approximations are often introduced due to the system complexity. Considering the lumped capacity modeling, Dobran [69] provided an interesting model that includes the thermohydraulics of the vapor core, liquid film, and liquid pool of the evaporator aiming to determine the steady-state characteristics and stability thresholds of a TPCT. He neglected the liquid film distribution along the wall, and assumed an averaged liquid film thickness. A parametric study was also performed to determine the effect of pipe geometry, FR, and working fluid properties on the operating limits. He only performed a linear analysis, thus, the theoretical results did not agree with the experimental data. Moreover, no physical mechanism was built into the model for predicting critical heat flux at low filling ratios. However, the work of [69] clearly defines a description of the various phenomena in a TPCT. Farsi et al. [70] improved the model proposed by [69] in order to analyze the transient regime of a TPCT (d_i=50 mm and L=300 mm). They analytically and experimentally investigated the effect of the heat flux, the inlet temperature of cooling water and the FR. Vieira da Cunha and Mantelli [71] presented a steady state lumped capacitance model to determine the design characteristics of a TPCT. In particular they focused on the analysis of the high temperature metal working fluid. Nusselt theory and nucleate boiling was considered for the liquid film condensed and the liquid pool, respectively. They found a great discrepancy with the correlation applied in the liquid pool region for sodium as a working fluid. Ziapour and Shaker [72] developed a simplified thermal network model for a TPCT based on the model of Zuo and Faghri [73]. It is a transient model that neglects the influence of the following; the fluid dynamics inside the pipe, the effect of gravity on inclined thermosyphons and the dependence of evaporation–condensation phase change on the saturation vapor temperature. They validated their model in both transient and steady regimes. Although the network model of [72] is simplified by considering several assumptions, the model could be improved by considering different expressions of condensation HTC [30-32], as shown in **Table 1**, and in this form could be useful for practical applications of tilted thermosyphons.

Concerning 1-D and 2-D numerical modeling of TPCTs, Pan [74] developed a condensation model of a TPCT by considering the interfacial shear due to mass transfer and interfacial velocity. They considered the relative

velocity ratio and the momentum transfer factor (the ratio of the interfacial shear with mass transfer to the interfacial shear without mass transfer) to describe the effects of vapor velocity and the mass transfer through the liquid-vapor interface (control the interfacial shear stress). The model predictions differ substantially from Nusselt's theory, showing the significance of the interfacial shear on the condensation inside the thermosyphon which compared with Nusselt's solution. They found that the relative velocity ratio and momentum transfer factor largely affect the condensation heat transfer in the thermosyphon. Harley and Faghri [75] presented a model which coupled a general quasi-steady Nusselt type solution of the falling film with the complete two-dimensional vapor solution to simulate the transient behavior of TPCT. A 2-D transient formulation for the vapor flow is coupled with transient heat conduction in the wall. The proposed model cannot predict the flooding limit, since the mass of the film was determined based on the vapor velocities to satisfy heat transfer requirements, and thus the mass of liquid is a function of heat input. Also, the falling film analysis is valid only for the FR that produces the liquid film with a zero film thickness at the condenser end cap and the evaporator end cap of the thermosyphon. They concluded that the Nusselt-type approximation can predict the condensation and evaporation HTC for low temperature TPCTs. Recently, Shabgard et al. [43] developed a two-dimensional numerical model to simulate the transient operation of a TPCT with various FRs. They have focused on the investigation of the thermal–hydraulic behavior of a TPCT in the underfilled, overfilled, and optimally-filled conditions, based on the numerical model for the condensate film which was developed by [75]. They simulated dynamic response of the condensate film and liquid pool and was coupled to the heat conduction in the wall and vapor flow. They found that the optimally-filled thermosyphon has the shortest response time and the lowest thermal resistance, even if, a slight increase in the input power causes a breakdown of the condensate film. In recent times, the researchers tried to simulation the TPCT using CFD and commercial codes. Fadhl et al. [76] built a CFD modelling to simulate the two-phase flow and heat transfer phenomena during the operation of a TPCT including the pool boiling in the evaporator section and the condensed liquid film in the condenser section. They reported that FLUENT with the VOF method can successfully model the complex phenomena inside the thermosyphon as good agreement between CFD predicted temperature profiles and experimental temperature data was observed.

Although, considerable studies have been undertaken to investigate the behavior of the TPCT in steady state situations, literature about their transient behavior have not been sufficiently investigated. An overview of the selected analytical and numerical studies including objectives, modes, operating limits (flooding and dryout), and some remarked consideration is shown in **Table 6.** As clearly indicated in **Table 6**, most of reviewed modeling approaches reviewed can be viewed as an extension to the Nusselt theory, take advantage of a number of simplifying assumptions such as the quasi-steady condensate liquid film. In some cases, key among these assumptions is the absence of shear on the interface, or neglecting the condensed liquid film, or neglecting the wall heat conduction, or just modeling condensation phenomena and in some cases the researchers considered the operating limits as boundary conditions (see **section 4**). The operation of a thermosyphon are very complex, thus it is not possible to compare various approaches because of the dependence of the models on the objective of the expected results. More fundamental works and accurate simulation of the liquid-vapor interface are needed to better understand the physical phenomena of TPCTs. Furthermore, an accurate experimental analysis appears to be important to design a TPCT for a specific application

6. TPCT: experimental devices

In this section the relevant experimental analysis on the TPCTs are reported. One of the important parameter affecting the TPCTs performance is the working fluid and the related filling ratio. Ong and Alalhi [77] investigated experimentally the effects of FR and ratio of evaporator on condenser lengths of a TPCT (d_i=25 mm and L=780 mm) using R-22, R-134a and water as working fluids. It was concluded that R-22 performed better than 134a for low operating temperature difference. Also, water performs better than R-22 and R-134a thermosyphons, but requires higher starting temperatures.

Terdtoon et al. [78] studied experimentally the internal flow patterns of thermosyphon and the effect of *AR* and *Bo* number on it at various angles. In addition they changed the FR (80-150%) using R123 as a working fluid. They concluded that at both higher and lower Bo with L_e/d_i<10, the internal flow patterns changed from bubble flow at vertical to slug flow at inclined positions (the cause of dryout is film boiling). But at L_e/d_i>10, annular flow at vertical changed to stratified flow at inclined positions (the cause of dryout is flooding). Abou-Ziyan et al. [79] experimentally investigated effect of vibration on a TPCT (d_i=23 mm and L=900 mm) using water and

R134a as a working fluid for different FRs (40-80%), adiabatic lengths, input heat fluxes (160-2800kW/m^2) and vibration frequencies. They observed the maximum performance TPCT for FR of 50%. They found that vibration can decrease the performance of TPCT using water as a working fluid from 5 up to 20%, below the boiling limit and less influence observed for R134a. Noie et al. [80] experimentally investigated the effect of the inclination angle (5–90˚) on the thermal performance of a TPCT (d_i=14.5 mm and L=1000 mm) using water as working fluid (FRs=15-30%) under normal operating conditions. The results show that the TPCT has the highest thermal performance in the inclination angle range of 15˚–60˚. They observed the geyser boiling for FRs of 30%. Jouhara and Robinson [81] experimentally investigated a stainless steel TPCT (d_i=6 mm and L=209 mm) using Therminol VP1 and Dowtherm A as the working fluid for medium-high temperature applications (200-450˚C). They observed thermal resistances of less than 0.4°C/W at working temperatures of up to 420°C corresponding with an axial heat flux of 2.5MW/m². Karthikeyan et al. [82] investigated the effect of inclination angle on the TPCT thermal performance. A TPCT (d_i=17 mm and L=1000 mm) was tested for different heat inputs of 40, 60 and 80 W and inclination angles of 45, 60 and 90˚. They concluded that the thermosyphon filled with the aqueous solution (n-Butanol) shows better thermal performance than the one charged with distilled water. Amatachaya and Srimuang [83] investigated the effects of cross-sectional geometries, FR and aspect ratio on thermal performance of thermosyphon at different rates of heat input. Two different cross-sectional geometries for the thermosyphon tube were used, one was circular and the other was flat tubular. The experimental results indicated that the flat TPCTs produced higher temperature values at the evaporator than for circular ones for the same heat input conditions. Tang et al. [84] experimentally and analytically analyzed the bubble flow regime and the operating liquid level in the evaporator of a TPCT (d_i=19 mm and L=1500 mm) considering influence of the dimension and condensation heat transfer. They showed that the suitable FR is 30–60%. Ordaz-Flores et al. [85] investigated the technical feasibility of a two-phase system using three working fluids: R134a, R410A and acetone. It was found that phase change system working with R134a and R410A has higher performance than acetone (about 20%). However, high pressure and some difficulties loading the working fluid have to be dealt with. Using acetone as working fluid was shown advantageous with regard to loading and low working pressure. Ong et al. [86] experimentally investigated a TPCT (d_i=32 mm and L=760 mm) using R410a and water at various filling ratios (25-100%), inclination angles (30-90˚) and power input ranges between 100–830 W. The

results showed that the evaporator wall temperature is not uniform especially at high power input, low FRs and large inclinations. Also, they found that the R410a filled thermosyphon performed better in the vertical position at all fill ratios and the water filled thermosyphon performed better at low fill ratio and when inclined. MacGregor et al. [87] experimentally investigated a TPCT (d_i=16 mm and L=2200 mm) with operating temperature ranges of 10-50˚C (cold side) and 60-80 ˚C for the hot side. They investigated different working fluids: water, methanol, ethylene glycol, and R-134a. They suggested that a water-5% ethylene glycol mixture was a suitable replacement fluid, although under certain conditions its performance was less than that of R134a. Jouhara et al. [88] experimentally tested a TPCT (d_i=20 mm and L=1500 mm) with an inclined condenser and horizontal evaporator section using two working fluids (water and ethanol-water). The results of this investigation demonstrated the ability of TPCT to operate at evaporator inclination angle from 0 to 90˚ which can be used for various applications such as the receivers of concentrated solar collectors. They have not found a clear effect of the inclination angle between 15 and 90˚. Zhang et al. [89] experimentally investigated the heat transfer performance of a stainless steel TPCT (d_i=43 mm and L=1525 mm) with different inclination angles (0-90˚) under low-temperature conditions. They showed that inclination angle has a significant impact on the heat transfer performance of a TPCT under the experimental conditions tested. The minimum total thermal resistance was observed at an inclination angle of approximately 20°, and approximately 0.76 times as much as that at the inclination angle of 90˚ and the maximum total thermal resistance observed at an inclination angle of approximately 80°, but only very slightly higher than at 90°.

Further, TPCTs have been fabricated with large length dimensions. Wu et al. [90] investigated a stainless steel TPCT with evaporator and condenser lengths of 3 and 2 m, respectively, using R134a as a working fluid for cooling data centers. A large length TPCT (d_i=11 mm and L=5000 mm) has been experimentally investigated by Zhang and Che [91]. They experimentally investigated also the applicability of the TPCT (L=17 m) in cyclic steam stimulation for heavy oils. They showed that the TPCT sucker rod can decrease the heat loss of fluids in wellbore and improve well performance during cyclic steam stimulation. Recently, Bolozdynya et al. [92] investigated a tubular cryogenic TPCT (d_i=11 mm and L=5000 mm) filled with nitrogen fluid. The system worked at temperature range of 80–120 ˚K with the heat transfer limit up to 100 W without mechanical vibrations.

Concerning the experimental analysis of TPCT, different efforts can be evidenced in order to enhance the TPCT performance. Some researchers used the surface modification strategy and other focused on using nanoparticle working fluid. In the first approach, the porous coating structure is included in the design of TPCT to postpone flooding and improve contact between the wall and the liquid. Rahimi et al. [93] experimentally investigated the effect of resurfacing on the evaporator and the condenser in a TPCT (d_i=20 mm and L=1100 mm). They observed an increase of about 15% of thermal performance by resurfacing the pipe wall. Recently, Solomon et al. [94] investigated heat transfer characteristics of an anodized TPCT (d_i=16 mm and L=350 mm) with refrigerant as the working fluid (R600a and R290) for the heat input ranges between 50–200 W. They showed that the total thermal resistance of the anodized TPCT can be reduced by 17%, 20% and 23%, respectively, for horizontal, inclined and vertical positions in comparison with non-anodized one.

Nanoparticles also can be used as a working fluid in a TPCT. Some of the experimental analyses on nanofluid are summarized as follow. Xue et al. [95] investigated the thermal performance of a TPCT (d_i=20 mm and L=500 mm) using carbon nanotube (CNT) suspension as a working fluid. They showed that the total heat resistance of the TPCT using CNT is higher than that of the one using pure water. Liu et al. [96] experimentally investigated the effect nanofluid (de-ionized water and CuO nanoparticles) on the thermal performance of a TPCT (d_i=6 mm and L=350 mm). They observed an enhancement of the boiling heat transfer performance in comparison of pure water. Liu et al. [97] further investigated the effect of using water-based carbon nanotube suspensions as the working fluid. They observed the optimal mass concentration is about 2.0% to achieve the maximum heat transfer enhancement. Khandekar et al. [98] investigated the effect of using water/Al2O3, CuO and laponite clay on a TPCT (d_i=16 mm and L=620 mm). They observed that the thermal performance of nanofluids is significantly influenced by alteration in the fluid/solid interface. Noie et al. [99] investigated the effect of using water/Al2O3 nanoparticles on a TPCT (d_i=20 mm and L=1000 mm). They showed the performance of the TPCT increases to about 15% by using Al2O3/water nanofluid in comparison of water. Parametthanuwat et al. [100] investigated the effect of using water/silver nanofluid on a TPCT (d_i=7.5, 11.1 and 25.4 mm). They suggested a correlation to predict the heat flux for the TPCT in the vertical position. Huminic et al. [101] experimentally investigated the effect of using water/iron oxide nanoparticles on a TPCT (d_i=13.5 mm and L=2000 mm). They investigated the effect of inclination angle ranges between (30˚-90˚) and showed the

maximum heat transfer enhancement of 19% in comparison of water. Buschmann and Franzke [102] investigated the effect of using water/TiO2 nanofluids on a TPCT (d_i=25 mm and L=500 mm). They showed a maximal reduction of 24% for thermal resistance in comparison of water as a working fluid. Recently, Heris et al. [103] investigated the thermal performance of oxidized carbon nanotubes (CNT)/water nanofluids in a TPCT. They showed a decrease on the mean temperature of the evaporator and condenser sections in comparison of water. In general, all the researchers observed that these nanofluids show: inferior thermal performance than pure fluid, enhanced thermal conductivities, an increase in CHF under pool boiling conditions and an increase in the performance of the TPCT. The reason for the performance enhancement depends on the heat transfer mechanism and thermo-physical properties of nanofluids. However, the results appear to be dispersed for heat transfer analysis and there is a need for further investigations in the field of nanofluids. Other TPCT configurations like as flat disc TPCTs [104] and rotating TPCTs [105], although already studied in the literature, are not considered in this review because is not specific interest in the considered applications.

7. TPCT: Applications

The TPCTs can be applied for several thermal control and energy storage applications. Interesting applications can be evidenced in the literature between solar collector and TPCTs. Figs. 8(a) and 8(b) show a flat plate and a concentrating solar collector, respectively where the TPCT is applied for heat transfer from a solid (absorbed solar radiation) to an external fluid flow as thermal energy. Abreu and Colle [18] focused on the experimental analysis of the thermal behaviour of TPCTs. The effects of evaporator lengths (1000, 1350 and 1500 mm), FRs (60% and 80%), cooling temperatures (20˚C and 40˚C) and slopes (30˚ and 45˚) on their performance were considered. Results showed that an increase of filling ratio from 60 to 80% lead to increase of the evaporator temperature especially at higher input heat fluxes. Nada et al. [106] experimentally investigated a TPCT-flat plate collector (FPC) with different water mass flow rates (0.01-0.06 kg/s), the inlet cooling water temperature and the number of the pipes (8-14). They found that there is an optimal operating point for the mass flow rate. The efficiency of the system under different flow rates ranges from 35 to 60%. Hussein et al. [107] experimentally investigated the effect of cross section geometry and the working fluid filing ratios (10, 20 and 30%) on the TPCT-FPC performance (d_i=18 mm and L=1500 mm). They showed that the elliptical cross

sections have better performance than the circular cross section at low filling ratios. Enaburekhan and Yakasai [108] investigated a TPCT-FPC using different working fluids: R-134a, R12, and ethanol. They observed different values of temperature increases of 28, 37 and 40°C and different values of the maximum efficiencies of 40, 51 and 57 for R12, ethanol and R-134a, respectively. Chow et al. [109] experimentally and numerically investigated the single phase open thermosyphon and the TPCT system performance applied in the evacuated tube solar water heaters. They found that the daily and annual thermal performance of the TPCT solar collector is 13% more than the single phase open thermosyphon. Samanci and Berber [110] experimentally compared performance between single-phase and TPCT (d_i=12 mm and L=1380 mm) solar water heater systems. Water was used as the working fluid for single phase and R-134a for two-phase. They found that, in particular, the efficiency increase obtained with TPCT is 43% more than the other one. Xiao et al. [111] analyzed and discussed the influences of relevant parameters on the thermal performance of TPCT-FPC. It was found that as the water mass flow rate increases, the thermal efficiency value increases and the highest thermal efficiency observed when number of tube is 12. Zhang et al. [112] experimentally investigated a TPCT (d_i=70 mm and L=2000 mm) system applied to a parabolic trough solar collector (PTC) with concentration ratio of 80. They showed that the system can generate steam of a pressure up to 0.75 MPa. The thermal efficiency was found to be about 40% at a discharging pressure of 0.5 MPa. Wei et al. [113] used a large integrated thermosyphon instead of side-by-side separate thermosyphons to improved structure of the FPCs. Ethanol was used as the working fluid with the FR of 50%. The experimental results showed that the maximum collector efficiency was about 66%. Chougule et al. [114,115] experimentally investigated a TPCT-FPC (d_i=10 mm and L=625 mm) using pure water, water-2-ethyl-hexanol surfactant and carbon nanotubes and various tilt angles (20-60˚). They showed the maximum efficiency of 73% using nanofluid (30% higher than using pure water) and the system efficiency increases with the tilt angle and decreases when the tilt angle exceeds 50˚. Mamouri et al. [116] investigated an evacuated collector desalination system using a TPCT (d_i=8 mm and L=2000 mm). They observed considerable increase in the production rate of desalinated water and system efficiency with a maximum production rate, but quite low value of the maximum efficiency, about 23%.

A second important application of TPCTs is gas to gas heat transfer for heat recovery systems in ventilation and air conditioning (HVAC) or in drying systems. Fig 8(c) and 8(d) show an example of application of TPCT in a

drying system and a HVAC system, respectively. Meyer and Dobson [117] experimentally investigated a TPCT-heat exchanger (HE) for a relatively small mini-drier. They found that in particular, with installing TPCT, the total drier power consumption reduces about 30%. Yau [118] experimentally investigated an eight-row TPCT-HE (d_i=15 mm) for tropical building HVAC systems. They investigated the sensible heat ratio of the system. They suggested that the tropical HVAC systems could be installed with TPCT-HE for dehumidification enhancement. Hagens et al. [119] presented an air–to-air TPCT-HE with two FRs (20% and 60%). They obtained the HTC of heat exchanger as 10–40 W/m^{2}K for evaporator section and 20-50 W/m^{2}K for the condenser section. Firouzfar et al. [120] experimentally investigated a TPCT-HE using methanol-silver nanofluid as a working fluid. They observed that the system can save around 9-32% for cooling and 18-100% for reheating the supply air stream in an air conditioning system. Byrne et al. [17] tested a TPCT (d_i=10 mm and L=750 mm) with R407C as working fluid for an air-source heat pump for heating and cooling of residential buildings. Ambient air was applied as a balancing source to run a heating or a cooling mode. Results showed an annual performance increase of 17% compared to a standard reversible heat pump. Jouhara and Merchant [121] investigated a nine finned TPCT-HE (d_i=16 mm and L=900 mm) using water as the working fluid. They predicted the effectiveness of the thermosyphon-HE under test. They observed that the HE provides optimal performance at vertical position for different heat inputs (750-1500 W). Danielewicz et al. [122] experimentally and analytically predicted the performance of an air-to-air TPCT-HE. They observed that there are an optimum number of rows to maximize efficiency of system. Meena et al. [123] experimentally investigated the enhancement of a steel TPCT-HE (d_i=17.5 mm and L=500 mm) with fins and without fins using distilled water and Cu-nanofluid (FR of 50% total volume) as a working fluid for temperature range of 60-80˚C. They found that the maximum value of system efficiency using nanofluid at 80˚C, about 40% (10% more that distilled water).

Although numerous works have been carried out in the field of low and medium temperature solar applications, there is a lack of general data on the thermal performance of thermosyphons because of the variety of applications proposed in the literature and operating parameters. To the authors knowledge, little attention has been paid to experimental study of TPCT applied in solar application in particular for medium-high temperature applications. It is not possible using the experimental data available in the literature to have a clear perspective

for defining criteria and guidelines to design TPCTs for specific application. **Table 7** summarizes different TPCT applications and their parameters from literature.

8. Conclusions

This paper presents the state of the art of TPCTs from different points of view: analytical, numerical and experimental. TPCTs can provide reliable and effective thermal control for energy conservation, energy recovery and renewable energy applications. Even if there are several advantages associated with using TPCTs in the energy field, TPCTs are under-investigated and analyzed especially in the case of compact and solar equipment. Analytical and numerical analysis of the TPCT is well developed and different elements are available to define heat transfer coefficients in various sections, operating limits under various operating conditions and operation of devices. However, successful adoption of TPCTs modeling requires not only the prediction of thermal performance especially in transient mode but also the analysis of critical elements, like maximum heat transport. From an experimental point of view it is clear that most of nucleate boiling correlations enable the prediction of the evaporation HTC within an acceptable error limit. The experiments and predictions of Nusselt theory considering entrainment are in accordance in the condenser section. Even if a lot of experimental results can be evidenced, the large variety of analysis is not useful in order to obtain general statements, due to different experimental conditions. Moreover, there are still some problems and challenges on the heat and mass transfer mechanism of TPCTs. Concerning the problem of the definition of an optimum FR, a large number of studies have been performed to understand operating limits especially at high FR. An optimum FR selection could improve the system performance due to lower thermal resistances and response times. Therefore, more experimental and numerical studies are needed to understand optimum FR for a thermosyphon. The study of TPCTs with a low FR is therefore a matter of interest. Experimental studies are needed to enhance the level of confidence in the prediction of the operating limit.

There are also some studies to enhance the TPCT performance based on the use of surface modification and on the use of nanofluids. There are still some problems and challenges on the mechanism of heat transfer enhancement and it is obvious that more research is needed in future in order to identify a new technique to improve the heat transport properties of nanofluids in TPCTs.

On the authors opinion, a comparison of TPCT with wicked HP and other two-phase devices such as TPLT could be matter of additional research activities. Lastly, concerning the application of the TPCTs, further investigation of working fluids, and different system configurations need to be studied. Most of the applications reviewed in the literature refer to TPCTs devices operating at temperature lower than 100˚C, for thermal control applications. A specific field of application seems to be the low-medium temperature solar applications.

References

[1] Reay DA, Kew P. Heat Pipes, 5th ed. Oxford, UK: Butterworth-Heinemann;2006.

[2] Faghri A. Heat Pipe Science and Technology. Philadelphia, PA: Taylor & Francis;1995.

[3] Vasiliev LL, Kakac S. Heat pipe and solid sorption transformation, fundamentals and practical applications. Taylor & Francis Group, LLC;2013.

[4] Franco A, Filippeschi S. Closed Loop Two-Phase Thermosyphon of Small Dimensions: a Review of the Experimental Results. Microgravity Scie Technology 2012; 24: 165-79.

[5] Filippeschi S. Comparison between miniature periodic two-phase thermosyphons and miniature LHP applied to electronic cooling equipment. Appl Therm Eng 2011:31(5):795–802.

[6] Franco A, Filippeschi S. Experimental analysis of Closed Loop Two Phase Thermosyphon (CLTPT) for energy systems. Exp Thermal Fluid Sci 2013;51:302–11.

[7] Sobhan CB, Rag RL, Peterson GP. A review and comparative study of the investigations on micro heat pipes. Int J Energy Res 2007;31:664–88.

[8] Di Marco P, Filippeschi S, Franco A, Jafari D. Theoretical Analysis of Screened Heat Pipes for Medium and High Temperature Solar Applications. J Phys Conf Ser 2014;547:012010.

[9] Peterson GP. Heat Pipes, Modeling, Testing, and Applications. John Wiley and Sons; 1994.

[10] Hakeem MA, Kamil M, Arman I. Prediction of temperature profiles using artificial neural networks in a vertical thermosiphon re-boiler. Appl Therm Eng 2008;28:1572–9.

[11] Cao Y, Gao M. Wickless network heat pipes for high heat flux spreading applications. Int J Heat Mass Transf 2002;45:2539–47.

[12] Sundaram AS, Bhaskaran A. Thermal Modeling of Thermosyphon Integrated Heat Sink for CPU Cooling. J Electronics Cooling Thermal Control 2011;1:15-21.

[13] Siedel S, Robinson AJ, Kempers R, Kerslake S. Development of a naturally aspired thermosyphon for power amplifier cooling. J Phys Conf Ser 2014;525:012007.

[14] Poulad ME, Fung A. Potential benefits from Thermosyphon-PCM (TP) integrated design for buildings applications in Toronto. In: Proceedings of eSim: The Canadian Conference on Building Simulation 2012:601-14.

[15] Zhang M, Lai Y, Zhang J, Sun Z. Numerical study on cooling characteristics of two-phase closed thermosyphon embankment in permafrost regions. Cold Reg Sci Technol 2011;65:203–10.

[16] Tundee S, Srihajong N, Charmongkolpradit S. Electric power generation from solar pond using combination of thermosyphon and thermoelectric modules. Energy Proc 2014;48:453–463.

[17] Chotivisarut N, Nuntaphan A, Kiatsiriroat T. Seasonal cooling load reduction of building by thermosyphon heat pipe radiator in different climate areas. Renew Energy 2012;38:188-94.

[18] Lee J, Ko J, Kim Y, Jeong S, Sung T, Han Y, Lee J-p, Jung S. Experimental study on the double-evaporator thermosiphon for cooling HTS (high temperature super-conductor) system. Cryogenics 2009;49:390–7.

[19] Byrne P, Miriel J, Lénat Y. Experimental study of an air-source heat pump for simultaneous heating and cooling – part 2: dynamic behavior and two-phase thermosiphon defrosting technique. Appl Therm Eng 2011;88:3072–8.

[20] Abreu SL, Colle S. An experimental study of two-phase closed thermosyphons for compact solar domestic hot-water systems. Sol Energy 2004;76:141-5.

[21] Akbarzadeh A, Wadowski T. Heat pipe-based cooling systems for photovoltaic cells under concentrated solar radiation. Appl Therm Eng 1995;16(1):81–7.

[22] Jouhara H, Robinson AJ. Experimental investigation of small diameter two phase closed thermosyphons charged with water, FC-84, FC-77 and FC-3283. Appl Therm Eng 2010;30(2–3):201–11.

[23] Franco A, Filippeschi S. Experimental analysis of heat and mass transfer in small dimension, two phase loop thermosyphons. Heat Pipe Sci Technol 2010;2:163–82.

[24] Rohsenow WM, Harnett JP, Ganic EN. Handbook of Heat Transfer Fundamentals. 2nd ed. New York: McGraw-Hill;1985.

[25] Rohsenow WM, A method of correlating heat-transfer data for surface boiling of liquids. Trans ASME 1952;74:969–76.

[26] Seban RA, Faghri A. Film condensation in a vertical tube with a closed top. Int J Heat Mass transf 1984;27:944–8.

[27] Chen SJ, Reed JG, Tien CL. Reflux condensation in a two-phase closed thermosyphon. Int J Heat Mass Transf 1984; 25:1587–94.

[28] Gross U. Reflux condensation heat transfer inside a closed thermosyphon. Int J Heat Mass Transf 1992;35(2):279–94.

[29] Collier JG, Thome JR. Convective Boiling and Condensation. 3rd ed. Oxford Science Publications;1996.

[30] Wang JCY, Ma Y. Condensation heat transfer inside vertical and inclined thermosyphons. J Heat Transf 1991;113:777–80.

[31] Fiedler S, Auracher H. Experimental and theoretical investigation of reflux condensation in an inclined small diameter tube. Int J Heat Mass Transf 2004;47:4031–43.

[32] Hussein HMS, Mohamad MA, El-Asfouri AS. Theoretical analysis of laminar-film condensation heat transfer inside inclined wickless heat pipes flat-plate solar collector. Renew Energy 2001;23:525–35.

[33] Hashimoto H, Kaminaga F. Heat transfer characteristics in a condenser of closed two-phase thermosyphon: effect of entrainment on heat transfer deterioration. Heat Transfer-Asian Res 2002;31(3):212–25.

[34] Oh S, Revankar ST. Complete condensation in a vertical tube passive condenser. Int Commun Heat Mass Transf 2005;32:593–602.

[35] Gross U, Philipp Ch. Conjugated shear stress and Prandtl number effects on reflux condensation heat transfer inside a vertical tube. Int J Heat Mass Transf 2006;49:144–53.

[36] Baojin Q, Li Z, Hong X, Yan S. Heat transfer characteristics of titanium/water two-phase closed thermosyphon. Energy Convers Manag 2009;50(9):2174–9.

[37] EL-Genk MS, Saber HH. Heat transfer correlations for small, uniformly heated liquid pools. Int J Heat Mass Transf 1998;41(2):261–74.

[38] Stephan K, Abdelsalam M. Heat transfer correlation for natural convection boiling. Int J Heat Mass Transf 1980;23:73-87.

[39] Imura H, Sasaguchi K, Kozai H. Critical heat flux in a closed two-phase thermosyphon. Int J Heat Mass Transf 1983;26(8):1181–8.

[40] Shiraishi M, Kikuchi K, Yamarcishi T. Investigation of heat transfer characteristics of a two phase closed hermosyphon. In: Proceedings of the Fourth International Heat Pipe Conference 1981:95–104.

[41] Chowdhury FMD, Kaminaga F, Goto K, Matsumura K. Boiling heat transfer in a small diameter tube below atmospheric pressure on a natural circulation condition. J Jpn Assoc Heat Pipe 1997;16:14–16.

[42] Kiatsiriroat T, Nuntaphan A, Tiansuwan J. Thermal performance enhancement of thermosyphon heat pipe with binary working fluids. Exp Heat Transf 2000;13(2):137–52.

[43] Shabgard H, Xiao B, Faghri A, Gupta R, Weissman W. Thermal characteristics of a closed thermosyphon under various filling conditions. Int J Heat Mass Transf 2014;70:91–102.

[44] Park YJ, Kang HK, Kim CJ. Heat transfer characteristics of a two phase closed thermosyphon to fill charge ratio. Int J Heat Mass Transf 2002;45:4655–61.

[45] Noie SH, Heat transfer characteristics of a two-phase closed thermosyphon. Appl Therm Eng 2005;25(4):495–506.

[46] Guo W, Nutter DW. An experimental study of axial conduction through a thermosyphon pipe wall. Appl Therm Eng 2009;29:3536–41.

[47] Pioro IL, Experimental evaluation of constants for the Rohsenow pool boiling correlation, Int J Heat Mass Transf 1999;42:2003–13.

[48] Pioro IL, Rohsenow W, Doerffer SS. Nucleate pool-boiling heat transfer. II: assessment of prediction methods. Int J Heat Mass Transf 2004;47:5045–57.

[49] Filippeschi S, Salvadori G. Transient analysis of boiling heat transfer in periodic drying out miniature pools. Int J Multiphase Flow 2008;34:1088–95.

[50] El-Genk MS, Saber HH. Determination of operation envelopes for closed, two-phase thermosyphons. Int J Heat Mass Transf 1999; 42(5):889–903.

[51] Jiao B, Qiu LM, Gan ZH, Zhang XB. Determination of the Operation Range of a Vertical Two-Phase Closed Thermosyphon. Heat Mass Transf 2012;48(6):1043-55.

[52] Tien CL, Chung KS. Entrainment limits in heat pipes. AIAA J 1979;17(6):643–6.

[53] Nejat Z. Maximum heat flux for countercurrent two phase flow in a closed end vertical tube. Int J Multiphase Flow 1981;7:321–5.

[54] Zuo ZJ, Gunnerson FS. Heat transfer analysis of an inclined two-phase closed thermosyphon. ASME J Heat Transf 1995;117(4):1073–75.

[55] Lin TF, Lin WT, Tsay YL, Wu JC. Experimental investigation of geyser boiling in an annular two phase closed thermosyphon. Int J Heat Mass Transf 1995;38(2):295–307.

[56] Kunkoro H, Rao YF, Fukuda K. An experimental study on the mechanism of geysering in a closed two phase thermosyphon. Int J Multiphase Flow 1995;21(6):1243–52.

[57] Abreu SL, Skiavine JA, Colle S. Working characteristics of a compact solar hot water system with heat pipes during startup and geyser boiling periods. In: Proceedings of 13 IHPC-International Heat Pipe Conferences, Shanghai, China, 2004.

[58] Khazaee I, Hosseini R, Noie SH. Experimental investigation of effective parameters and correlation of geyser boiling in a two-phase closed thermosyphon. Appl Therm Eng 2010;30:406–12.

[59] Jiao B, Qiu LM, Zhang XB, Zhang Y. Investigation on the effect of filling ratio on the steady state heat transfer performance of a vertical two-phase closed thermosyphon. Appl Therm Eng 2008;28:1417–26.

[60] Faghri A, Chen MM, Morgan M. Heat transfer in two phase closed conventional and concentric annular thermosyphon. Int J Heat Mass Transf 1989;111:611–8.

[61] Katto Y, Hirao T. Critical heat flux of counter-flow boiling in a uniformly heated vertical tube with a closed bottom. Int J Heat Mass Transf 1991;34:993-1001.

[62] Golobic I, Gaspersic B. Corresponding states correlation for maximum heat flux in two-phase closed thermosyphon. Int J Ref 1997;20(6):402-10.

[63] Nakano A, Shiraishi M, Nishio M, Murakami M. An experimental study of heat transfer characteristics of a two-phase nitrogen thermosyphon over a large dynamic range operation. Cryogenics 1998;38:1259–66.

[64] Payakaruk T, Terdtoon P, Rittidech S. Correlations to predict heat transfer characteristic of an inclined closed two-phase thermosyphon at normal operating conditions. Appl Therm Eng 2000;20:781–90.

[65] Liu Z-h, Liao L, Zhang T. Critical heat flux of countercurrent boiling in an inclined small tube with closed bottom. Int Commun Heat Mass Transf 2008;35:995–1000.

[66] Rittidech S, Srimuang W. Correlation to predict heat-transfer characteristics of a vertical flat thermosyphon (VFT) at normal operating conditions. Int J Heat Mass Transf 2010;53:5984–7.

[67] Grooten MHM, Van Der Geld CWM. The Effect of the Angle of Inclination on the Operation Limiting Heat Flux of Long R-134a Filled Thermosyphons. ASME J Heat Transf 2010;132/051501-1.

[68] Long ZQ, Zhang P. Experimental investigation of the heat transfer characteristics of a helium cryogenic thermosyphon. Cryogenics 2013;57:95–103.

[69] Dobran F. Steady-state characteristics and stability thresholds of a closed two-phase thermosyphon. Int J Heat Mass Transf 1985;28(5):949–57.

[70] Farsi H, Joly JL, Miscevic M, Platel V, Mazet N. An experimental and theoretical investigation of the transient behavior of a two-phase closed thermosyphon. Appl Therm Eng 2003;23:1895–1912.

[71] Vieira da Cunha AF, Mantelli MBH. Analytical and experimental analysis of a high temperature mercury thermosyphon. J Heat Transf 2009;131(9):1-7.

[72] Ziapour BM, Shaker H. Heat transfer characteristics of a two-phase closed thermosyphon using different working fluids. Heat Mass Transf 2010;46:307–14.

[73] Zuo ZJ, Faghri A. A network thermodynamic analysis of the heat pipe. Int J Heat Mass Transf 1997;41:1473–84.

[74] Pan Y. Condensation heat transfer characteristics and concept of sub-flooding limit in a two-phase closed thermosyphon. Int Commun Heat Mass Transf 2001;28(3):311–22.

[75] Harley C, Faghri A. Complete Transient Two-Dimensional Analysis of Two-Phase Closed Thermosyphons Including the Falling Condensate Film. J Heat Transf 1994;116(2):418-26.

[76] Fadhl B, Wrobe LC, Jouhara H. Numerical modelling of the temperature distribution in a two-phase closed thermosyphon. Appl Therm Eng 2013;60:122-31.

[77] Ong KS, HMD Alalhi. Experimental investigation on hysteresis effect in vertical two phase closed thermosyphons. Appl Therm Eng 1999;19:399–408.

[78] Terdtoon P, Waowaew N, Tantakom P. Internal flow patterns of an inclined, closed two-phase thermosyphon at critical state: case study 2, effect of Bond number. Exp Heat Transf 1999:359–73.

[79] Abou-Ziyan HZ, Helali A, Fatouh M, Abo El-Nasr MM. Performance of stationary and vibrated thermosyphon working with water and R134a. Appl Therm Eng 2001;21:813-30.

[80] Noie SH, Sarmasti Emami MR, Khoshnoodi M. Effect of Inclination Angle and Filling Ratio on Thermal Performance of a Two-Phase Closed Thermosyphon under Normal Operating Conditions. Heat Transfer Eng 2007;28(4):365–71.

[81] Jouhara H, Robinson AJ. An experimental study of small-diameter wickless heat pipes operating in the temperature range 200ºC to 450ºC. Heat Transfer Eng 2009;30(13):1041–48.

[82] Karthikeyan M, Vaidyanathan S, Sivaraman B. Thermal performance of a closed thermosyphon using aqueous solution. Int J Eng Sci 2010;2:913-8.

[83] Amatachaya P, Srimuang W. Comparative heat transfer characteristics of a flat two-phase closed thermosyphon (FTPCT) and a conventional two-phase closed thermosyphon (CTPCT). Int Commun Heat Mass Transf 2010;37:293–8.

[84] Tang Z-w, Han Y-f, Liu A-j, Song W-g. Modeling analysis of bubble flow regime in a closed two-phase thermosyphon. Heat Mass Transf 2011;47:1685–9.

[85] Ordaz-Flores A, García-Valladares O, Gómez VH. Experimental characterisation and technical feasibility of a closed two-phase vs a conventional solar water heating thermosyphon. Appl Therm Eng 2011;31:1313-22.

[86] Ong KS, Tong WL, Gan JS, Hisham N. Axial temperature distribution and performance of R410 and water thermosyphon at various fill ratios and inclinations. Front Heat Pipes 2014;5:2.

[87] MacGregor RW, Kew PA, Reay DA. Investigation of low Global Warming Potential working fluids for a closed two-phase thermosyphon. Appl Therm Eng 2013;51:917-25.

[88] Jouhara H, Ajji Z, Koudsi Y, Ezzuddin H, Mousa N. Experimental investigation of an inclined-condenser wickless heat pipe charged with water and an ethanolewater azeotropic mixture. Energy 2013;61:139-47.

[89] Zhang M, Lai Y, Pei W, Jin L. Effect of inclination angle on the heat transfer performance of a two-phase closed thermosyphon under low-temperature conditions. J Cold Reg Eng 2014;28(4):04014007-1.

[90] Wu XP, Mochizuki M, Mashiko K, Nguyen T, Nguyen T, Wuttijumnong V, et al. Cold energy storage systems using heat pipe technology for cooling data centers. Front. Heat Pipes 2011;2: 013005.

[91] Zhang X, Che H. Reducing heat loss of fluids in heavy oil wellbore using two-phase closed thermosyphon sucker rod. Energy 2013;57:352-8.

[92] Bolozdynya AI, Dmitrenko VV, Efremenko YV, Khromov AV, Shafigullin RR, Shakirov AV, Sosnovtsev VV, Tolstukhin IA, Uteshev ZM, Vlasik KF. The two-phase closed tubular cryogenic thermosyphon. Int J Heat Mass Transf 2015;80:159–62.

[93] Rahimi M, Asgary K, Jesri S. Thermal characteristics of a resurfaced condenser and evaporator closed two-phase thermosyphon. Int. Commun. Heat Mass Transfer 2010;37:703–10.

[94] Solomon AB, Roshan R, Vincent W, Karthikeyan VK, Asirvatham LG. Heat transfer performance of an anodized two-phase closed thermosyphon with refrigerant as working fluid. Int. J. Heat Mass Transfer 2015;82:521–29.

[95] Xue HS, Fan JR, Hu YC, Hong RH, Cen KF. The interface effect of carbon nanotube suspension on the thermal performance of a two-phase closed thermosyphon. J. Appl Physics 2006:100;104909.

[96] Liu Z-h, Yang X-f, Guo G-l. Effect of nanoparticles in nanofluid on thermal performance in a miniature thermosyphon. J Appl Phys 2007;102:013526.

[97] Liu Z-h, Yang X-f, Wang G-s, Guo G-l. Influence of carbon nanotube suspension on the thermal performance of a miniature thermosyphon. Int J Heat Mass Transf 2010;53:1914–20.

[98] Khandekar S, Joshi YM, Mehta B. Thermal performance of closed two-phase thermosyphon using nanofluids. Int J Therm Sci 2008;47:659–67.

[99] Noie SH, Zeinali Heris S, Kahani M, Nowee SM. Heat transfer enhancement using Al2O3/water nanofluid in a two-phase closed thermosyphon. Int J Heat Fluid Flow 2009;30:700–5.

[100] Parametthanuwat T, Rittidech S, Pattiya A. A correlation to predict heat-transfer rates of a two-phase closed thermosyphon (TPCT) using silver nanofluid at normal operating conditions. Int J Heat Mass Transf 2010;53:4960–5.

[101] Huminic G, Huminic A, Morjan I, Dumitrache F. Experimental study of the thermal performance of thermosyphon heat pipe using iron oxide nanoparticles. Int J Heat Mass Transf 2011;54:656–61.

[102] Buschmann MH, Franzke U. Improvement of thermosyphon performance by employing nanofluid. Int J Ref 2014;40:416–28.

[103] Heris SZ, Fallahi M, Shanbedi M, Amiri a. Heat transfer performance of two‐phase closed thermosyphon with oxidized CNT/water nanofluids. Heat Mass Transfer 2015:10.1007.

[104] Zhang M, Liu Z, Ma G. The experimental investigation on thermal performance of a flat two-phase thermosyphon. Int J Thermal Sci 2008;47:1195–203.

[105] Waowaew N, Terdtoon P, Maezawa S, Kamonpet P, Klongpanich W. Correlation to predict heat transfer characteristics of a radially rotating heat pipe at vertical position. Appl Thermal Eng 2003;3:1019–32.

[106] Nada SA, El-Ghetany HH, Hussein HMS. Performance of a two-phase closed thermosyphon solar collector with a shell and tube heat exchanger. Appl Therm Eng 2004;24:1959–68.

[107] Hussein HMS, El-Ghetany HH, Nada SA. Performance of wickless heat pipe flat plate solar collectors having different pipes cross sections geometries and filling ratios. Energy Convers Manag 2006;47:1539-49.

[108] Enaburekhan J, Yakasai UT. Performance evaluation of a refrigerant-charged integrated solar water heater in northern Nigeria. Desalination 2009;243:208–17.

[109] Chow TT, Dong Z, Chan LS, Fong KF, Bai Y. Performance evaluation of evacuated tube solar domestic hot water systems in Hong Kong. Energy Build 2011:43:3467–74.

[110] Samanci A, Berber A. Experimental investigation of single-phase and two phase closed thermosyphon solar water heater systems. Sci Res Essays 2011;6(4):688-93.

[111] Xiao L, Wu SY, Zhang QL, Li YR. Theoretical investigation on thermal performance of heat pipe flat plate solar collector with cross flow heat exchanger. Heat Mass Transf 2012; 48:1167-76.

[112] Zhang L, Wang W, Yu Z, Fan L, Hua Y, Ni Y, Fan J, Cen K. An experimental investigation of a natural circulation heat pipe system applied to a parabolic trough solar collector steam generation system. Sol Energy 2012;86911–9.

[113] Wei L, Yuan D, Tang D, Wua B. A study on a flat-plate type of solar heat collector with an integrated heat pipe. Sol Energy 2013; 97:19–25.

[114] Chougule SS, Sahu SK, Pise AT. Performance Enhancement of Two Phase Thermosyphon Flat-Plate Solar Collectors by Using Surfactant and Nanofluid. Front Heat Pipes 2013;4:013002.

[115] Chougule SS, Sahu SK, Pise AT. Thermal Performance of Two Phase Thermosyphon Flat-Plate Solar Collectors Using Nanofluid. J Sol Energy Eng 2014;136:014503-1.

[116] Mamouri SJ, Derami HG, Ghiasi M, Shafii MB, Shiee Z. Experimental investigation of the effect of using thermosyphon heat pipes and vacuum glass on the performance of solar still. Energy 2014;75:501-7.

[117] Meyer A, Dobson RT. A heat pipe heat recovery heat exchanger for a mini-drier. J Energy South Afr 2006;17:50-7.

[118] Yau YH. Application of a heat pipe heat exchanger to dehumidification enhancement in a HVAC system for tropical climates-a baseline performance characteristics study. Int J Therm Sci 2007;46:164–71.

[119] Hagens H, Ganzevles FLA, Van Der Geld CWM, Grooten MHM. Air heat exchangers with long heat pipes: experiments and predictions. Appl Therm Eng 2007;27:2426-34.

[120] Firouzfar E, Soltanieh M, Noie SH, Saidi SH. Energy saving in HVAC systems using nanofluid. Appl Therm Eng 2011;31:1543-5.

[121] Jouhara H, Merchant H. Experimental investigation of a thermosyphon based heat exchanger used in energy efficient air handling units. Energy 2012;39:82-9.

[122] Danielewicz J, Sayegh MA, Sniechowska B, Szulgowska-Zgrzywa M, Jouhara H. Experimental and analytical performance investigation of air to air two phase closed thermosyphon based heat exchangers. Energy 2014;77:82-7.

[123] Meena P, Tammasaeng P, Kanphirom J, Ponkho A, Setwong S. Enhancement of the Performance Heat Transfer of a Thermosyphon with Fin and without Fin Heat Exchangers Using Cu-Nanofluid as Working Fluids. J Eng Thermophysics 2014;23(4)331–40.

"Figures 1-8"

Fig. 1 A schematic of TPCT system.

Fig. 2 (a) Schematic of a TPCT and (b) thermal network model and the expression of resistances

Fig. 3 Comparison of the experimentally and theoretically determined HTC values for the evaporator section of the: (a) water (HTC<10 kW/m^2K), (b) ethanol, TEG, R134a and FC72 (HTC< 10 kW/m^2K), and (c) water, ethanol and R113 (HTC>20 kW/m^2K) (see **Table 3** to find each case (C)).

Fig. 4 Comparison of the experimentally and theoretically determined HTC values for the condenser section of the TPCT: (a) water (b) ethanol, TEG, R134a and R113, see **Table 3** to find each case (C).

Fig.5 Flow patterns inside a TPCT [59].

Fig. 6 Comparison between the experimental and predicted heat fluxes (see **Tables 3** and **5** to find details).

Fig. 7 The ratio of maximum heat transfer versus Bond number at the flooding limit (see **Tables 3 and 5** to find details).

Fig. 8 schematic view of TPCT applications (a) flat plate solar collector (b) concentrating collector (c) dryer system (d) HVAC system.

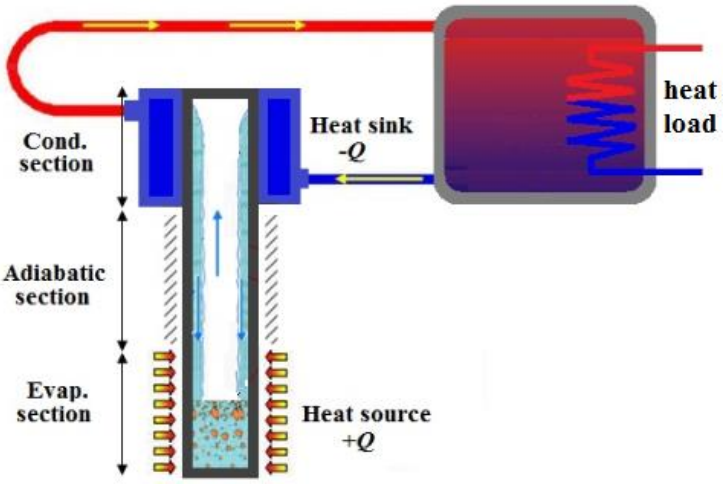

Fig. 1 A schematic of TPCT system.

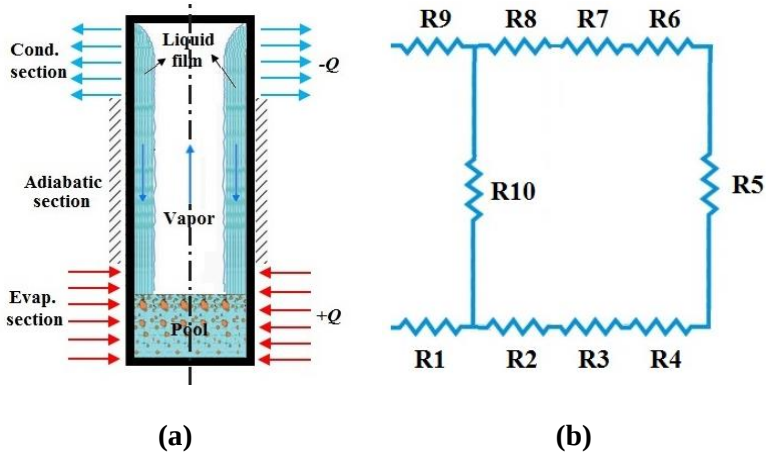

(a) **(b)**

R1: the Evap. external thermal resistance,
R9: the Cond. external thermal resistance,
R2: the heat conduction through the wall (Evap./radial),
R10: the heat conduction through the wall (adiabatic/axial),
R8: the heat conduction through the wall (Cond./radial),
R3: the evaporation thermal resistance,
R7: the condensation thermal resistance,
R5: the vapor thermal resistance,
R4: the liquid vapor interface thermal resistance (Evap.),
R6: the liquid vapor interface thermal resistance (Cond.).

$$R2=\frac{\ln(d_o/d_i)}{2\pi L_e k_w},\ R10=\frac{L_{eff}}{1/4\,\pi(d_o^2-d_i^2)k_w},\ R8=\frac{\ln(d_o/d_i)}{2\pi L_c k_w},\ R3=\frac{1}{\pi d_i h_e L_e},\ R7=\frac{1}{\pi d_i h_c L_c},$$

$$R5=\frac{128 L_t R_g \mu_v (T_{v,e}-T_{v,c}/2)^2}{\pi d_i^4 h_{fg}^2 P_v \rho_v},\ R4=\frac{R_g T^2 (2\pi R_g T)^{1/2}}{\pi d_i L_e h_{fg}^2 P_v},\ R6=\frac{R_g T^2 (2\pi R_g T)^{1/2}}{\pi d_i L_c h_{fg}^2 P_v}$$

Fig. 2 (a) Schematic of a TPCT and (b) thermal network model and the expression of resistances

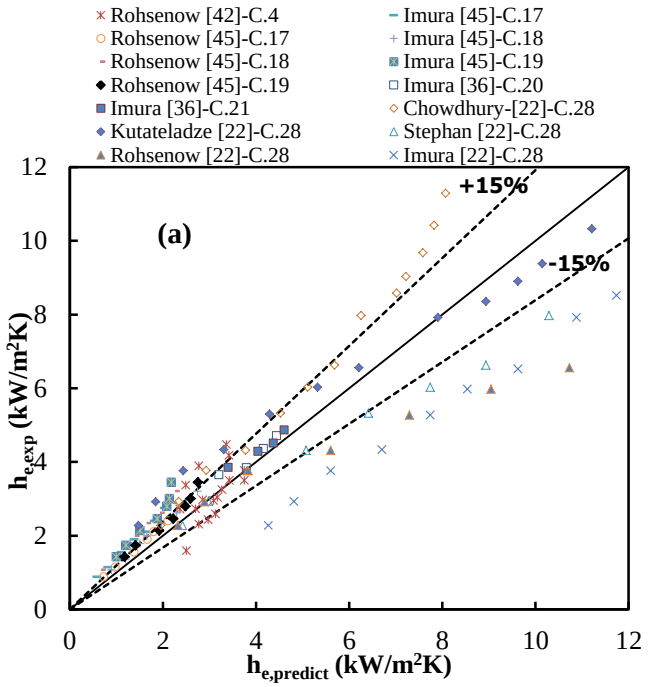
Rohsenow [42]-C.4
Imura [45]-C.17
Rohsenow [45]-C.17
Imura [45]-C.18
Rohsenow [45]-C.18
Imura [45]-C.19
Rohsenow [45]-C.19
Imura [36]-C.20
Imura [36]-C.21
Chowdhury-[22]-C.28
Kutateladze [22]-C.28
Stephan [22]-C.28
Rohsenow [22]-C.28
Imura [22]-C.28
(a)
+15%
-15%
$h_{e,exp}$ (kW/m^{2}K)
$h_{e,predict}$ (kW/m^{2}K)
0
2
4
6
8
10
12

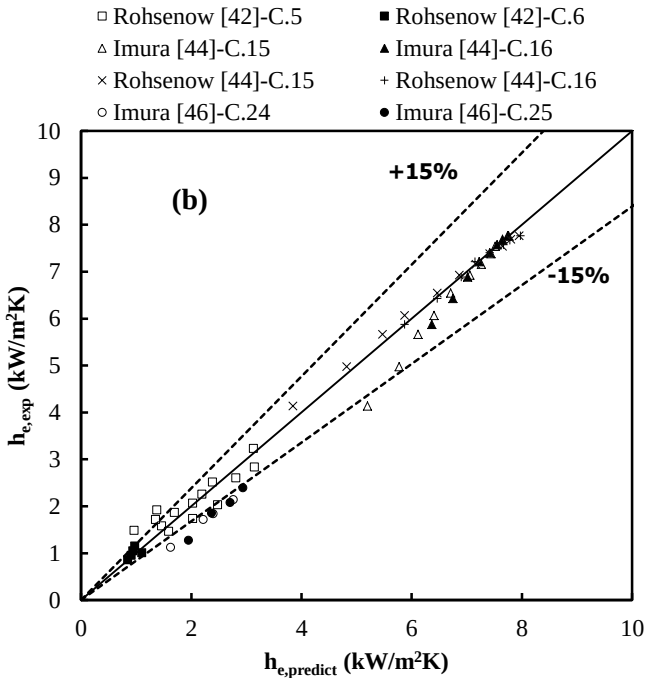
Rohsenow [42]-C.5
Rohsenow [42]-C.6
Imura [44]-C.15
Imura [44]-C.16
Rohsenow [44]-C.15
Rohsenow [44]-C.16
Imura [46]-C.24
Imura [46]-C.25
(b)
+15%
-15%
$h_{e,exp}$ (kW/m^{2}K)
$h_{e,predict}$ (kW/m^{2}K)
0
1
2
3
4
5
6
7
8
9
10

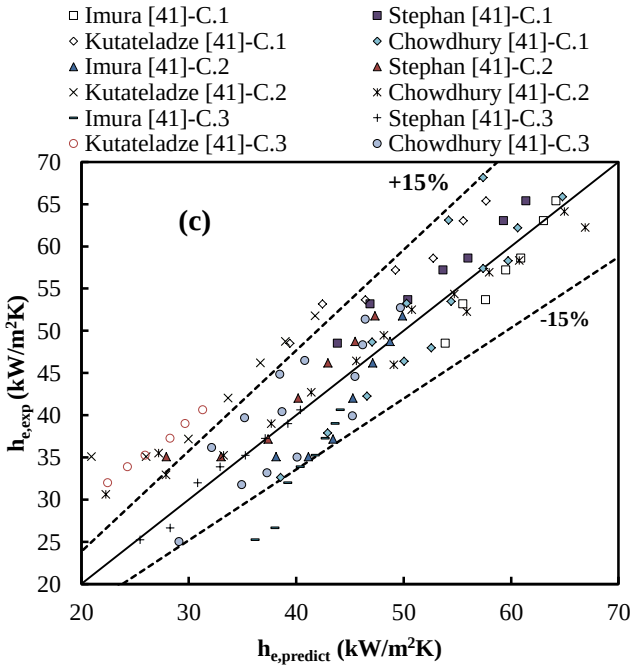

Fig. 3 Comparison of the experimentally and theoretically determined HTC values for the evaporator section of the: (a) water (HTC<10 kW/m^{2}K), (b) ethanol, TEG, R134a and FC72 (HTC< 10 kW/m^{2}K), and (c) water, ethanol and R113 (HTC>20 kW/m^{2}K) (see **Table 3** to find each case (C)).

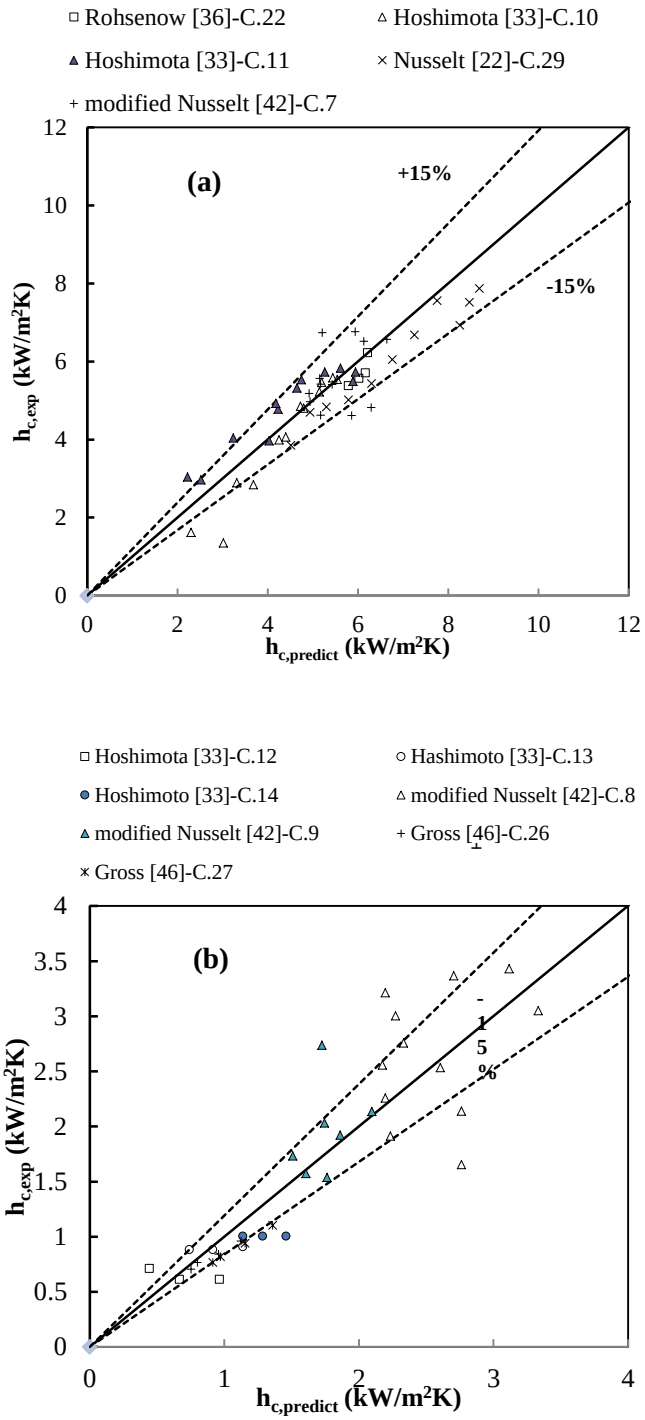

Fig. 4 Comparison of the experimentally and theoretically determined HTC values for the condenser section of the TPCT:

(a) water (b) ethanol, TEG, R134a and R113 (see **Table 3** to find each case (C)).

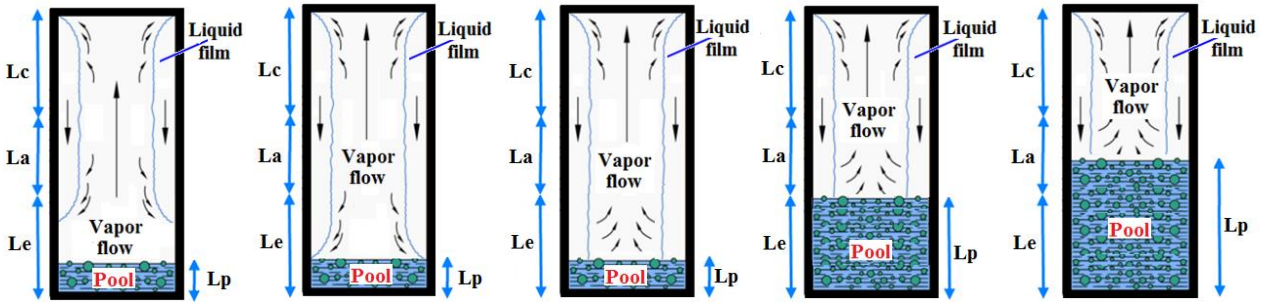

(a) dryout liquid film | (b) minimum value of liquid film thickness | (c) continuous liquid film and liquid pool | (d) liquid pool fills entire evaporator | (e) liquid pool exceeds evaporator

Fig.5 Flow patterns inside a TPCT [59].

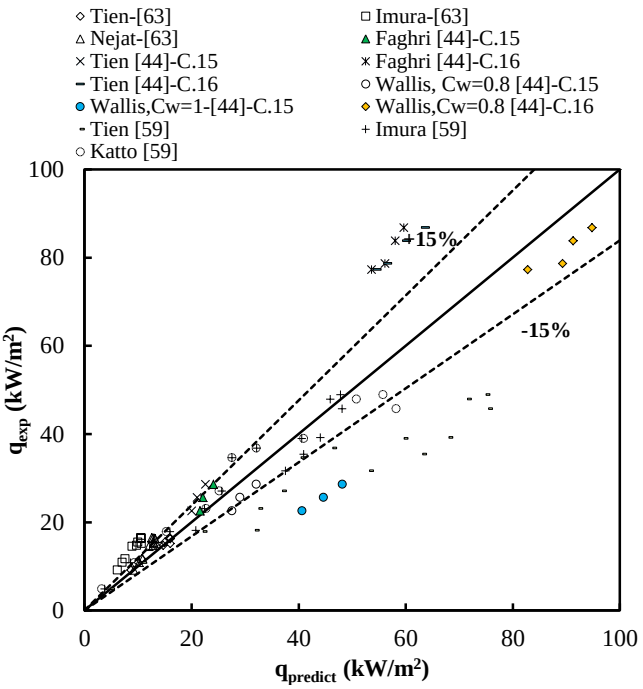

Fig. 6 Comparison between the experimental and predicted heat fluxes (see **Tables 3 and 5** to find details).

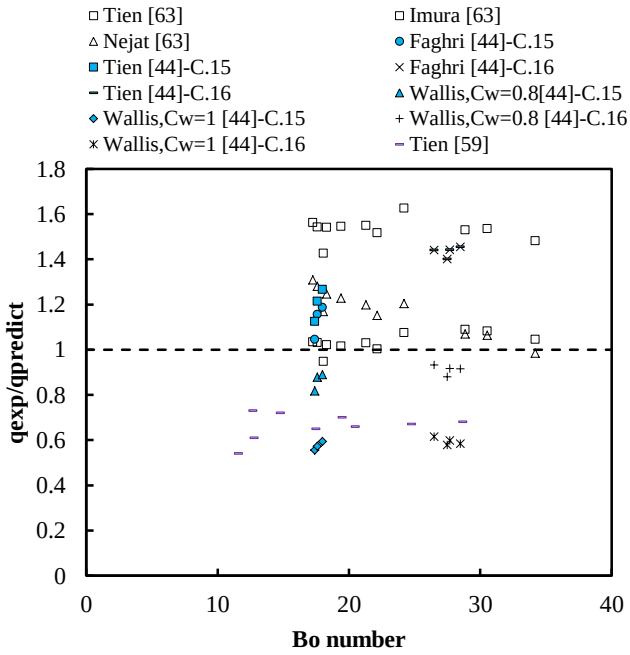

Fig. 7 The ratio of maximum heat transfer versus Bond number at the flooding limit (see **Tables 3** and **5** to find details).

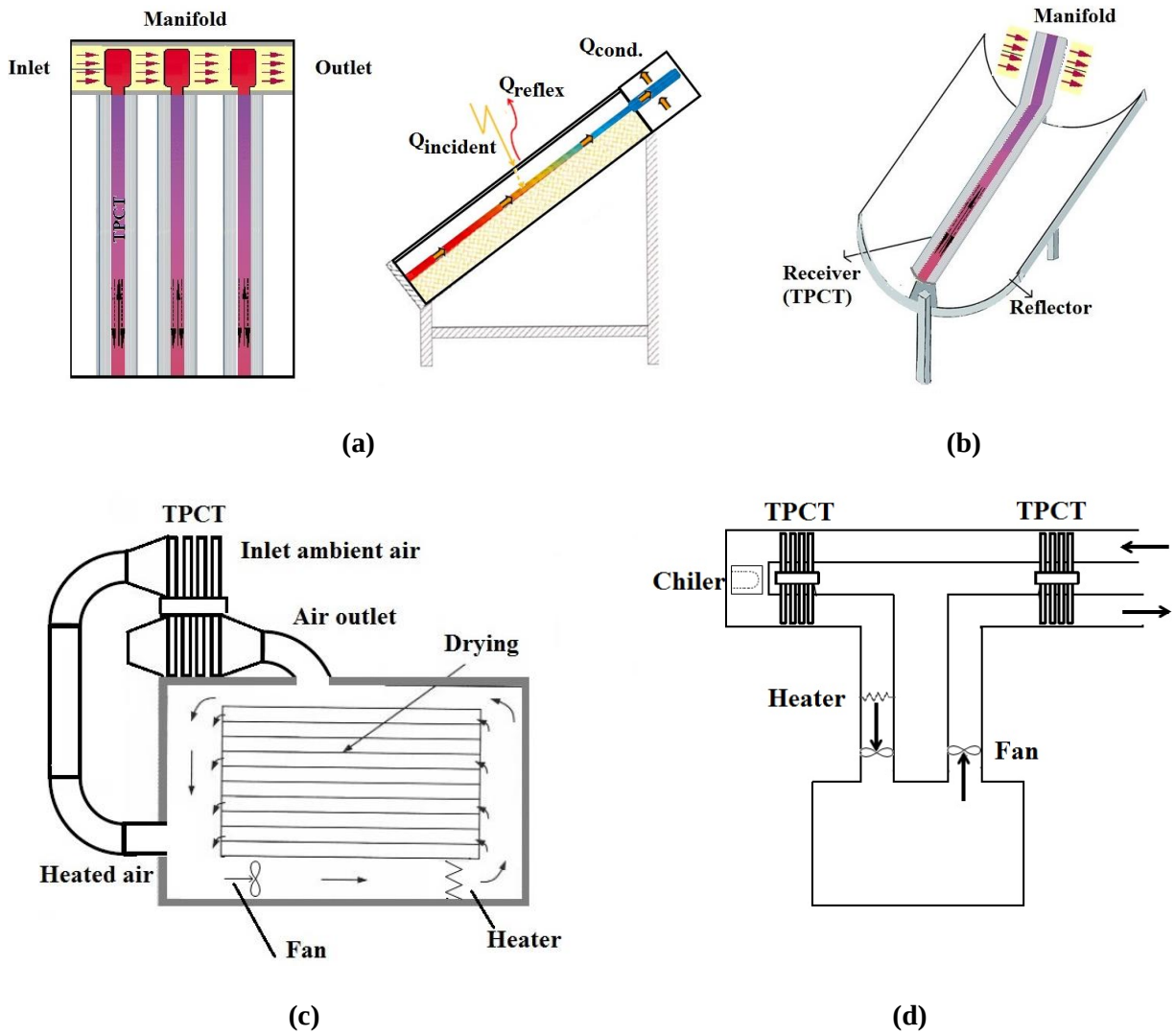

Fig. 8 schematic view of TPCT applications (a) flat plate solar collector (b) concentrating collector (c) dryer system (d) HVAC system.

“Tables 1-7”

Table 1 A lists of some correlations provided for the calculation of condensation HTC

Table 2 A lists of some correlations provided for the calculation of evaporation HTC

Table 3 Experimental data references of heat transfer coefficient in the TPCT

Table 4 A lists of some correlations provided by various researchers for the calculation of various TPCT limits

Table 5 Experimental data references of operating limit in the TPCT

Table 6 Previous analytical and numerical studies of TPCTs and remarked consideration

Table 7 Applications of TPCT and their parameters

Table 1 A lists of some correlations provided for the calculation of condensation HTC

Correlations	References
$h_{Nusselt} = 0.943\left\{\frac{\rho_l(\rho_l-\rho_v)gk_l^3\left[h_{fg}+0.68C_{pl}(T_v-T_c)\right]}{\mu_l(T_v-T_c)L_c}\right\}^{1/4}$	Nusselt theory in [24]
dimensionless form: $Nu^* = 0.925\,\mathrm{Re}^{-1/3}{}_{\max,l}$, $(\mathrm{Re}_{\max,l} < 325)$	
$\mathrm{Re}_{\max,l} = Q/\pi d\mu_l h_{fg}$, $Nu^* = h_c L^*/k_l$, $L^* = \left[v_l^2/g(\rho_l/\rho_l-\rho_v)\right]^{1/3}$	
$h_c = 1.509 h_{Nusselt}\left(\frac{P_v}{P_{crit}}\right)^{0.14}$	Rohsenow in [24]
$Nu_{Gross}{}^* = \left[\left(0.925\,f_d\,\mathrm{Re}^{-1/3}{}_{\max}\right)^2 + \left(0.044\,\mathrm{Pr}^{2/5}\,\mathrm{Re}^{1/6}{}_{\max}\right)^2\right]^{1/2}$ (	Gross [28]
$Nu_{Gross}{}^* = h_c L^*/k_l$)	
$f_d = \left[1-0.63(P/P_{crit})^{3.3}\right]^{-1}$, (enhancement factor)	
$h_c = h_{Nusselt}\left(\frac{L_c}{r_i}\right)^{\cos(\beta/4)}\left[0.54+\left(5.68\times10^{-3}\beta\right)\right]$	Wang and Ma [30]
$h_c = h_{Nusselt}\left(\frac{L_c}{r_i}\right)^{\cos(\beta/4)}\left[0.125+\left(1.46\times10^{-2}\beta\right)-\left(7.27\times10^{-5}\beta^2\right)\right]$	Fiedler and Auracher [31]
$h_c = h_{Nusselt}\left(\frac{L_c}{d_i}\right)^{1/4(\cos\beta)^{0.358}}\left[0.997-0.334(\cos\beta)^{0.108}\right]$	Hussein et al. [32]
$h_c = 0.85\,\mathrm{Re}_f^{0.1}\exp\left(-0.000067\frac{\rho_l}{\rho_v}-0.6\right)h_{Nusselt}$	Hashimoto and Kaminaga [33]
$h_c = 0.85\,\mathrm{Re}_f^{0.1}\exp\left(-0.000067\frac{\rho_l}{\rho_v}-0.14\right)h_{Nusselt}$	Jouhara and Robinson [22]

Table 2 A lists of some correlations provided for the calculation of evaporation HTC

Correlations	References
$he = 0.32\left(\frac{\rho_l^{0.65} k_l^{0.3} C_{pl}^{0.7} g^{0.2}}{\rho_v^{0.25} h_{fg}^{0.4} \mu_l^{0.1}}\right)\left(\frac{P_v}{P_{atm}}\right)^{0.3} q^{0.4}$	Imura et al. [39]
$h_e = 0.44\,\mathrm{Pr}^{0.35}\left(\frac{k_l}{L_b}\right)\left(\frac{\rho_l}{\rho_l-\rho_v}\frac{qP\times10^{-4}}{\rho_v g h_{fg}\mu_l}\right)^{0.7}$	Kutateladze in [24]
$h_e = 0.32\left(\frac{\rho_l^{0.65} k_l^{0.3} C_{pl}^{0.7} g^{0.2}}{\rho_v^{0.25} h_{fg}^{0.4} \mu_l^{0.1}}\right)\left(\frac{P_v}{P_{atm}}\right)^{0.23} q^{0.4}$	Shiraishi et al. [40]
for water: $h_e = 11.43(\mathrm{Re}_b)^{0.72}(\mathrm{Pr}_l)^{0.42}\left(\frac{\rho_v}{\rho_l}\right)^{0.5}\left(\frac{d_b}{d_i}\right)\left(\frac{k_l}{d_b}\right)$ for ethanol: $h_e = 495.7(\mathrm{Re}_b)^{0.8}(\mathrm{Pr}_l)^{0.5}\left(\frac{\rho_v}{\rho_l}\right)^{0.33}\left(\frac{k_l}{d_b}\right)$ For Freon R-113: $he = 6(\mathrm{Re}_b)^{0.78}(\mathrm{Pr}_l)^{0.48}\left(\frac{\rho_v}{\rho_l}\right)^{0.58}\left(\frac{k_l}{d_b}\right)$, $\mathrm{Re}_b = \frac{qd_b}{\rho_v h_{fg} v_l}$	Chowdhury et al. [41]
water: $h_e = 0.246\times10^7\left(\frac{qd_b}{k_l}\right)^{-0.327}\left(\frac{h_{fg}d_b^2}{\alpha_l}\right)^{-1.58}\left(\frac{C_p T_{sat} d_b}{\alpha_l}\right)^{0.5}\left(\frac{\rho_l-\rho_v}{\rho_l}\right)^{5.22}$ ammonia: $h_e = 207\left(\frac{qd_b}{k_l T_{sat}}\right)^{-0.255}\left(\frac{\rho_v}{\rho_l}\right)^{0.581}\left(\frac{v_l}{\alpha_l}\right)^{0.533}$	Stephan and Abdelsalam [38]
$\frac{C_p\Delta T}{h_{fg}} = C_{s,f}\left(\frac{qL_b}{\mu h_{fg}}\right)\left(\frac{C_p}{\mu k_l}\right)^n$, where $h_e = q/\Delta T$, $C_{s,f}$ is the constant, and n is the power (see Pioro, 1999#[45]).	Rohsenow in [24]
$h_e = C\left(\frac{\mu h_{fg}}{L_b\Delta T}\right)\left(\frac{C_p\Delta T}{h_{fg}\,\mathrm{Pr}}\right)^n$, where C is 18.688, 17.625 and 20.565 and n is 0.3572, 0.3300 and 0.3662 for water, ethanol and TEG, respectively.	Kiatsiriroat et al. [42]
$h_e = \Psi(1+4.95)0.44\left(\frac{k_l}{L_b}\right)\left(\frac{10^{-4}qP}{g\rho_v h_{fg}\mu_l}\frac{\rho_l}{\rho_l-\rho_v}\right)^{0.7}\mathrm{Pr}_l^{0.35}$ $\Psi = \left(\frac{\rho_v}{\rho_l}\right)^{0.4}\left[\frac{P_v v_l}{\sigma}\left(\frac{\rho_l^2}{\sigma g(\rho_l-\rho_v)}\right)^{1/4}\right]^{1/4}$	El-Genk and Saber [37]

Table 3 Experimental data references of heat transfer coefficient in the TPCT

Refs.	Dimensions (mm) D= d_o / d_i L= $L_t / L_e / L_c$	L_e/d_i	Heat flux (kW/m^2)	HTC	Case (C)	Material/fluid(FR%)	HTF (W/m^2K)	R (K/W)
[41]	D=n.a/2.8 L=150/50/50	17.8	9-90	Evap.	1	SS/Water (n.a.)	48510-65375	0.047-0.035
					2	SS/ethanol (n.a)	35100-51700	0.065-0.044
					3	SS/R113 (n.a.)	25250-40620	0.09-0.05
[42]	D=25/21 L=100/40/40	1.9	0-470	Evap.	4	SS/water (50)	1600-4470	0.23-0.084
					5	SS/ethanol (50)	1470-3220	0.25-0.11
					6	SS/TEG (50)	850-1140	0.44-0.33
				Cond.	7	SS/water (50)	4620-6760	0.081-0.056
					8	SS/ethanol (50)	1915-3430	0.20-0.11
					9	SS/TEG (50)	1540-2740	0.24-0.14
[33]	D=n.a./19.5 L=995/431/384	22.1	3-370	Cond.	10	SS/Water (30)	1620-5590	0.026-0.007
					11	SS/Water (50)	2960-5800	0.014-0.007
					12	SS/R113 (30)	610-710	0.07-0.06
					13	SS/Ethanol (30)	880-910	0.048-0.046
					14	SS/ethanol (30)	1000	0.042
[44]	D=22/19 L=600/105/420	5.5	4-80	Evap.	15	Cu/FC72 (10)	4130-7760	0.038-0.020
					16	Cu/FC72 (70)	5870-7760	0.027-0.020
[45]	D=32/25 L=980/314/380	12.5	3-29	Evap.	17	Cu/water (30)	880-2750	0.046-0.014
					18	Cu/water (60)	1075-3210	0.037-0.012
					19	Cu/water (90)	1430-3450	0.028-0.011
[36]	D=25/22.5 L=1000/350/350	15.5	12-24	Evap.	20	Cu/water (36)	3650-4710	0.011-0.0085
					21	Ti/water (36)	3850-4860	0.010-0.0083
				Cond.	22	Cu/water (36)	5375-6200	0.0075-0.0065
					23	Ti/water (36)	13500-16200	0.003-0.0025
[46]	D=28.5/26 L=770/250/240	9.6	1-10	Evap.	24	Cu/R134a (65)	1115-2130	0.043-0.022
					25	Cu/R134a (85)	1270-2390	0.038-0.020
				Cond.	26	Cu/R134a (45)	700-960	0.072-0.053
					27	Cu/R134a (85)	770-1100	0.066-0.046
[22]	D=12/6 L=200/40/60	6.6	15-170	Evap.	28	Cu/Water (160)	2280-12840	0.58-0.103
				Cond.	29	Cu/water (80)	2850-7870	0.23-0.11

n.a: not available

Table 4 A lists of some correlations provided by various researchers for the calculation of various TPCT limits

Limits	Correlation	Ref.
Flooding	$Q_{ent} = f_1(Bo)\, f_2\, f_3(Bo,\beta) h_{fg} \left(\pi r_i^2\right) \rho_v^{1/2} \left[g(\rho_l - \rho_v)\sigma\right]^{1/4}$	[1]
	f_1 is a function of Bo; $\begin{cases} f_2 = K_p^{-0.17}, K_p \le 4\times10^4 \\ f_2 = 0.165, K_p \ge 4\times10^4 \end{cases}$, $K_P = \dfrac{P_v}{\left[g(\rho_l - \rho_v)\sigma\right]^{1/2}}$	
	$f_3 = 1,\ \beta = 90^\circ$; f_3 is a function of Bo for tilted position	
	$Q_{ent} = \xi(\pi r_i^2) h_{fg} (\rho_l^{-1/4} - \rho_v^{-1/4})^{-2} \left[\sigma g(\rho_l - \rho_v)\right]^{1/4}$	
	$\xi = C_w 3.2^{1/2} \tanh^2 Bo^{1/4}$, $0.8 < C_w < 1$	Wallis in [2]
	$\xi = C_w 3.2^{1/2} \tanh^2 0.25 Bo^{1/4}$, $C_w = 1$	Tien and Chung [52]
	$\xi = \left(\dfrac{\rho_l}{\rho_v}\right)^{0.14} \tanh^2 Bo^{1/4}$	Faghri et al. [60]
	$Q_{ent} = 0.14\left(1 - \dfrac{T_s}{T_c}\right)^{1/5} Bo^{0.5} \dfrac{(d_i/L_e)^{0.9}}{\left[1 + (\rho_v/\rho_l)^{0.25}\right]^2} h_{fg} \rho_v^{0.5} \left[\sigma g(\rho_l - \rho_v)\right]^{0.25}$	Kutateladze in [2]
	$Q_{ent} = \dfrac{d_i}{4L_e} \left(\dfrac{L_e}{d_i}\right)^{0.1} \dfrac{0.36 Bo^{0.5}}{\left[1 + (\rho_v/\rho_l)^{0.25}\right]^2}$	Nejat 1981 [53]
	$Q_{ent} = 0.32\left(\dfrac{\rho_l}{\rho_v}\right)^{0.13} \left(\dfrac{r_i}{L_e}\right) h_{fg} \left[\sigma g \rho_v^2 (\rho_l - \rho_v)\right]^{1/4}$	Imura et al. [39]
	$Q_{ent} = \dfrac{0.10 Bo^{0.3}}{1 + 0.491(L/D)}$	Katto and Hirao [61]
	$Q_{ent} = q_{ent,Ku} h_{fg} \rho_v^{0.5} \left[\sigma g(\rho_l - \rho_v)\right]^{0.25} \left[1 + \left(\lambda_1 \dfrac{T_s}{T_c} + \lambda_2\right)\beta\right]$;	Grooten and van der Geld [67]
	$\alpha_1 = -0.0125$ and $\alpha_2 = 1.01$	
Boiling	$Q_{boil} = 0.142 \rho_v^{1/2} \left[\sigma g(\rho_l - \rho_v)\right]^{1/4} \left[A' \left(\dfrac{d_i}{L_c}\right)^{-0.44} \left(\dfrac{d_i}{L_e}\right)^{0.55} \left(\dfrac{V_p}{V_e}\right)^{n'}\right]^2 \left\{0.4 + 0.012 r_i \left[\dfrac{g(\rho_l - \rho_v)}{\sigma}\right]^{1/2}\right\}^2$	[2]
	$A' = 0.538$ and $n' = 0.13$ for $\dfrac{V_p}{V_e} \le 35\%$; $A' = 3.54$ and $n' = -0.37$ for $\dfrac{V_p}{V_e} \ge 35\%$	
	$Q_{boil} = 0.12(2\pi r_i) h_{fg} \rho_v^{1/2} \left[\sigma g(\rho_l - \rho_v)\right]^{1/4}$	[1]
	$Q_{boil} = A''\left(\pi r_i^2\right) P_v^{0.22} L_e^{A'''}$ for $\dfrac{V_p}{V_e} \ge 4.5\%$	[51]
	A'' =20.8× 10^6, A''' = 0 at Le > 0.6 m and d_i > 27 mm;	
	A'' = 16 × 10^6, A''' = 0 at Le > 0.6 m and d_i <27 mm;	
	A'' = 24.4 × 10^6, A''' = 0.33 at Le<0.6 m.	
Dryout	$Q_{dry} = \dfrac{\pi g d_c \rho_l^2 h_{fg}}{3\mu} \left\{\dfrac{V_e(V_p/V_e - \rho_v/\rho_l)}{[\pi d_c(0.8L_c + L_a) + (d_e/d_c)^{2/3}(L_a + 0.75L_c)][1 - (\rho_v/\rho_l)]}\right\}^3$	[7]
Viscous	$Q_{vis} = \pi r_v^4 h_{fg} \dfrac{\rho_v P_v}{16 \mu_v L_{eff}}$	[7]
Sonic	$Q_{son} = \left(\pi r_i^2\right) \rho_v h_{fg} \left[\dfrac{\gamma R_v T_v}{2(\gamma + 1)}\right]^{1/2}$	[1]

Table 5 Experimental data references of operating limit in the TPCT

Ref.	**Dimensions (mm)** **D=** d_o / d_i **L=** $L_t / L_e / L_c$	Material	Working fluid	FR	Q (kW/m^2)	Limit
[55]	D=32/30 L=550/140,190/310	stainless steel	Water. ethanol	30-140	0.5-4	Geyser boiling
[63]	D=8.5/8 L=270/75/160	stainless steel	Nitrogen	100	5-80	Flooding
[64]	D=7.5, 11.1, 25.4/n.a L=Variable	copper	R22, R123, R134a, E, water	50, 80 and 100		flooding
[66]	Flat- 8.6 L= Variable	stainless steel	R123, ethanol and water	20-80	10-100	Flooding
[58]	D=17, 27/15, 24 L=1000/430/410	copper	Methanol	30-100	4-8	Geyser boiling
[67]	D=16/14.5 L=3000/1200/1450	copper	R134a	25	15	flooding
[51]	D=6/4 L=200/50/50	stainless steel	water	30-140	10-70	Dryout, boiling and flooding
[68]	D=14/10 L=270/70/150	copper	helium	10-150	0-8	dryout

Table 6 Previous analytical and numerical studies of TPCTs and remarked consideration

Ref.	Objective	Mode	Marked Study details and Consideration			
			limits		Liquid Pool	Modeling
			flooding	dryout		
[69]	operating limits	S	✓	×	✓	1-D, Lumped capacitance, neglected the distribution of liquid film (assumed that the liquid film can be represented by an average film thickness).
[54]	tilt Angle, working fluid inventory,	S	✓	✓	✓	1-D vapor flow and liquid flow, the shear stresses on liquid–vapor interfacial. Liquid film, liquid film and vapor include 3 cases based on inclination.
[32]	tilt Angle	S	×	×	×	2D-lumped capacitance, laminar film condensation.
[71]	high temperature (the working fluid)	S	×	×	✓	1-D, Lumped capacitance, a TPCT divided into three regions (evaporator, condenser and adiabatic sections). The adiabatic section is subdivided into two volumes (the liquid film and the vapor nucleus). The evaporator section is divided three volumes (the liquid film, the vapor nucleus region and the liquid pool). NB is considered for HTC of evaporation.
[72]	heat transfer characteristics	T	×	×	×	1D-Network model: three heat conduction processes (radial direction in condenser and evaporator section and axial direction in adiabatic section) and three heat convection processes (convection into pool, evaporation and condensation), without considering vapor flow and liquid film resistance.
[27]	operating limit	S	✓	×	×	Modified friction factors on the condensate film for the effect of mass transfer on interfacial shear stress.
[75]	pulsed response, film thickness	T	×	×	×	2D Vapor flow and solid wall, 1-D Liquid flow (quasi-steady, Nusselt-type), Valid only to predict critical FR (zero film thickness at two end of pipe).
[50]	dimension, power input	S	✓	✓	✓	1D, The operation is an enclosure with three boundaries (dryout, boiling and flooding limit), NC, TPC, NB are considered for HTC of evaporation.
[74]	interfacial shear on the condensation	S	✓	×	×	The interfacial shear due to mass transfer and interfacial velocity. A sub-flooding limit was proposed to capture the interaction between the condensation and evaporation.
[59]	FR	S	×	✓	✓	1-D, liquid film Nusselt type with sub-cooling of liquid film and interfacial shear stress between liquid film and vapor flow. Three types of flow pattern and two types of transition, also NC, NB are considered for HTC of evaporation.
[76]	thermal performance	S	×	×	✓	VOF technique, defined a UDF to simulate the mass and heat transfer between the liquid and vapor phases.
[43]	FR	T	×	✓	✓	2-D vapor flow and solid wall, 1-D liquid film (quasi-steady, Nusselt-type) as well as entrainment effects (condenser section), NC, TPC, NB, TPC-NB are considered for HTC of evaporation.

Table 7 Applications of TPCT and their parameters

Ref.	Application	Operating T or Q	HTF	material	**Dimensions (mm)** **D=** d_o / t **L=** $L_t / L_e / L_c$	FR	Parameter investigated
[18]	FPC	70 ˚C 0.2-1.2 kW/m^2	water	copper	D= 15/13.5 L=(1400-2000)/ 1000-1500/n.a	60 and 80%	evaporator length; filling ratio, inclination, cooling temperature
[106]	FPC	50-60 ˚C 0.8 kW/m^2	water	copper	D= 12.7/0.5 L= 920/750/100	n.a.	mass flow rate, cooling temperature, pipe number
[107]	FPC	50-60 ˚C 0.8 kW/m^2	water	copper	D=12.7/0.5 L= 920/750/100		cross section
[108]	FPC	0.4-0.9 kW/m^2	R-134a, R12, and ethanol	copper	D=2.5 L=1000	70 gr	working fluid
[110]	FPC	50-60 ˚C	R-134a	copper	D= 12.7/11.7 L= 1380/n.a/n.a	36% of (total ength)	single phase and two-phase systems
[111]	FPC	50-60 ˚C 0.75 kW/m^2	water	copper	D=12.7/n.a L=920/750/100	n.a.	pipe number
[112]	PTC	150-160 ˚C	water	stainless steel	D=70/n.a L=n.a/2000/n.a	70%	working conditions (Pressure)
[115]	FPC	50-60 ˚C 1.1 kW/m^2	water-Nano-fluid (CNT)	copper	D=12/1 L=625/510/85	60%	tilt Angle, working fluid
[117]	HE	40-60 ˚C	R134a	copper	D=16/n.a L=700/350/350	50%	thermal performance
[119]	HE	40-70 ˚C	R134a	copper	D=16/0.8 L=1500/640/640	20-60%	mass flow rate, inlet and outlet Tem., operating limit
[120]	HVAC	7 kW	methanol-silver nanofluid	copper	D=16/1 L=1560/	50%	working fluid
[122]	HE	60-120 ˚C	methanol	carbon steel	D=27/3.5 L=2200/1000/1000		condenser and evaporator inlet mass flow rates

n.a: not available